Geochimica et Cosmochimica Acta 337 (2022) 106–122

Contents lists available at ScienceDirect

Geochimica et Cosmochimica Acta

journal homepage: www.elsevier.com/locate/gca

Concentration-runoff relationships of contrasting small mountainous rivers in the Pacific Northwest, USA: Insights into the weathering of rhenium relative to other weathering products

Layla Ghazi [a,*], Miguel Goñi [a], Brian A. Haley [a], Jesse M. Muratli [a], Julie C. Pett-Ridge [a,b]

[a] College of Earth, Ocean, and Atmospheric Sciences, Oregon State University, Corvallis, OR, USA
[b] College of Agricultural Sciences, Department of Crop and Soil Sciences, Oregon State University, Corvallis, OR, USA

ARTICLE INFO

Article history:
Received 19 April 2022
Accepted 26 September 2022
Available online 1 October 2022
Associate editor: Lixin Jin

Keywords:
Dissolved chemistry
Concentration-runoff
Concentration-discharge
Rhenium

ABSTRACT

This study examines dissolved rhenium (Re) concentrations as a function of water runoff using river samples from two contrasting mountainous watersheds, the Eel and Umpqua Rivers in the Pacific Northwest, USA. These watersheds share many key characteristics in terms of size, discharge, climate, and vegetation, but they have a 15-fold difference in sediment yield due to differences in their tectonic setting and uplift and erosion rates. We evaluate concentration-runoff (C-R) relationships and ratios of coefficients of variation (CV_C/CV_R) for major cations, anions, dissolved inorganic carbon, selected trace elements including Re, and $^{87}Sr/^{86}Sr$ ratios. Recent research outlines the potential of Re to serve as a tracer for the oxidation of ancient/fossil organic matter because of its close association with petrogenic carbon (OC_{petro}) in rocks. In both the Eel and Umpqua Rivers, our measurements show that Re behaves similarly to major weathering derived-solutes corrected for atmospheric input, such as Ca^{2+*}, Mg^{2+*}, and Na^{+*} with modest dilution across all tributaries with increasing runoff. Rhenium behaves dissimilarly from other trace elements, such as Mo and U, and is also dissimilar to biologically-cycled nutrients, such as NO_3^-, PO_4^{3-}, and K^{+*}, suggesting differences in sources, solute generation mechanisms, and flowpaths. Rhenium behavior is also distinct from that of colloids, which have increasing concentrations with increasing runoff. We find that Re and sulfate corrected for atmospheric input (SO_4^{2-*}) have distinct C-R relationships, in which SO_4^{2-*} undergoes greater dilution with increasing runoff. This implies that Re is not dominantly sourced from sulfide weathering, which leaves primary bedrock minerals and OC_{petro} hosted in bedrock of these watersheds as the likely dominant sources of dissolved Re release. At mean discharge, Re concentration in the Eel river (3.5 pmol L^{-1}) is more than two times greater than Re concentrations in the Umpqua River (1.5 pmol L^{-1}). Furthermore, comparison of two tributary watersheds with similar bedrock but marked differences in erosion rates show higher Re concentrations in Bull Creek (erosion rate of 0.5 mm yr^{-1}) relative to Elder Creek (erosion rate of 0.2 mm yr^{-1}). The results of this study suggest that dissolved Re in the Eel and Umpqua River basins is likely derived from primary mineral dissolution or OC_{petro} oxidation, and Re fluxes are higher in areas with higher erosion rates, suggesting that tectonic setting is one factor that controls Re release and therefore OC_{petro} oxidation.

1. Introduction

On geologic timescales, Earth's carbon cycle is governed by five processes: (1) silicate weathering by carbonic acid; (2) the burial of biogenic organic carbon; (3) volcanic emissions; (4) weathering of carbonates via sulfuric acid; and (5) the oxidation of organic carbon stored in sedimentary rocks (also known as petrogenic organic carbon, or OC_{petro}), in a process called geologic respiration or georespiration (Hilton and West, 2020). The estimated global reservoir size of sedimentary OC_{petro} is 12.5×10^9 PgC, compared to 0.04×10^9 PgC in the combined ocean, atmosphere, plus biosphere reservoir, and compared to 65.3×10^9 PgC in calcium carbonate (Copard et al., 2007; Hilton and West, 2020; Husson and Peters, 2017). Over geologic timescales, georespiration is one of the major sources of CO_2 emissions into the atmosphere and sinks of O_2 that has not yet been well quantified.

The majority of Earth's OC_{petro} reservoir is stored in shale rocks, thus studies that examine the weathering of OC_{petro} have focused on analysis of shale weathering profiles (Bolton et al., 2006; Jaffe

* Corresponding author.
E-mail address: ghazil@oregonstate.edu (L. Ghazi).

https://doi.org/10.1016/j.gca.2022.09.036
0016-7037/

et al., 2002; Longbottom and Hockaday, 2019; Petsch, 2014; Petsch et al., 2000; Wildman et al., 2004). The major findings of these studies and others is that the depletion of OC_{petro} during shale weathering is potentially due to (i) microbial assimilation, (ii) dissolution of OC_{petro} to DOM, (iii) oxidation of OC_{petro} to CO_2 gas, and (iv) loss of OC_{petro} as the particulate (POC_{petro}) during physical erosion. Carbon isotope analysis in phospholipid fatty acids provides evidence for microbial assimilation of shale-derived OM by heterotropic, autropic, aerobic, and anerobic organisms, indicating both abiotic and biotic use of OC_{petro} (Petsch et al., 2001). During weathering, OC_{petro} may also be released as dissolved organic carbon (Chang and Berner, 1999; Wengel et al., 2006). Most studies assume that the dominant loss pathway for OC_{petro} is gaseous CO_2 (Hemingway et al., 2018; Soulet et al., 2021).

The supply of oxygen at depth during weathering is ultimately controlled by erosion, therefore, it follows that rate of CO_2 release during georespiration is controlled by the rate of physical erosion that brings OC_{petro} into the weathering environment and exposes the OC to oxidation (Bolton et al., 2006; Galy et al., 2008; Galy et al., 2015; Hilton et al., 2014). Once OC_{petro} is oxidized to CO_2 gas, it is very difficult to trace in an open system, thus there are large uncertainties regarding the magnitude of calculated global georespiration fluxes (Keller and Bacon, 1998). Some studies suggest that if erosion is a dominant control on how much OC_{petro} is available, a first order approximation of determining OC_{petro} oxidation would lie in the comparison of the change between upstream and downstream OC_{petro} in the particulate phase of the suspended sediment (Bouchez et al., 2010; Galy et al., 2015). This approach can be challenging in complex watersheds with variable OC_{petro} distributions and compositions. Radiocarbon techniques have helped further constrain and identify biogenic or petrogenic carbon in the sediment loads of some rivers. However, the limitation with measuring ^{14}C of riverine suspended sediment is that the measurement only shows how much unoxidized OC_{petro} is transported from upstream in the watershed downstream to the point of measurement, as opposed to how much georespiration has occurred.

The redox-sensitive element rhenium (Re) is a promising tracer for the weathering of OC_{petro} (Hilton et al., 2014; Horan et al., 2019; Horan et al., 2017; Jaffe et al., 2002). Under oxic conditions, dissolved Re is present as the soluble oxyanion perrhenate (ReO_4^-), which is stable across a wide range of pH (0–14) and Eh (0.3–1 V) conditions and is thought to behave conservatively in rivers, estuaries, and oxic ocean environments (Anbar et al., 1992; Brookins, 1986; Colodner et al., 1993; Sheen et al., 2018). Perrhenate is stable across a wider range of Eh and pH than other trace element oxides in freshwater (Brookins, 2012). Rhenium is removed from solution under extremely reducing conditions (Dolor et al., 2009; Helz and Dolor, 2012), thus Re may be enriched in ocean sediments with organic matter and mineral surfaces, which eventually form sedimentary rocks rich in OC_{petro} like shales (Cohen et al., 1999; Colodner et al., 1995; Dolor et al., 2009; Pierson-Wickmann et al., 2002; Rooney et al., 2012; Selby and Creaser, 2003). When these marine sedimentary rocks are eventually re-exposed to the surface through tectonic processes, georespiration occurs, rendering Re associated with OC_{petro} subject to oxidative chemical weathering. Thus, the release of dissolved Re thought to occur concomitantly with the release of CO_2 from OC_{petro} rich rocks (Dalai et al., 2002; Hilton et al., 2014; Horan et al., 2019; Jaffe et al., 2002). Little is known about the specific mechanisms controlling the release of Re and OC_{petro}, but the use of the Re tracer relies heavily on the observation that Re solubility is highly dependent on O_2 presence within the typical range of Eh-pH conditions for weathering at the Earth's surface.

In solid phases, Re is geochemically considered a chalcophile, a siderophile, and an organophile element (Rooney et al., 2012). Thus, questions remain whether Re release in terrestrial weathering environments is entirely associated with OC_{petro} oxidation, or if dissolved Re reflects dissolution of sulfide minerals, which are also known to host Re and are commonly present in the same marine sedimentary rocks (Miller et al., 2011). The average concentration of Re in the upper continental crust is estimated to be 0.4 ng g^{-1} (McLennan, 2001). In their assessment of the global cycling of Re in the near surface environment, Miller et al. (2011) concluded that the global average pre-anthropogenic Re concentration in rivers is 11.2 pmol kg^{-1}. Some evaluations of compiled global river chemistry have observed a positive correlation between dissolved Re and SO_4^{2-}, and have interpreted this as reflecting a common source, likely sulfide weathering (Colodner et al., 1993; Dalai et al., 2002; Miller et al., 2011; Rahaman et al., 2012). In addition, there is some uncertainty whether or not Re may be a trace component of silicate minerals (Dalai et al., 2002; Dellinger et al., 2021). In their study of Re isotopic fractionation, Dellinger et al. (2021) found in sequential extractions of Mackenzie River basin shale, the highest proportion of Re was measured in the organic-plus-sulfide fraction (62–69% of total Re), and <7% of Re was hosted in the silicate fraction, although some silicate was removed in other extraction steps. End-member mixing analysis of Re/Na^+ and Re/SO_4^{2-} ratios from the Mackenzie River, the Ehrlenbach and Vogelbach Rivers in the Swiss Alps, and the East River in Colorado, USA suggest a dominant role of OC_{petro} oxidation in supplying dissolved Re, relative to sulfide or silicate phases, but there is considerable uncertainty in the end-member compositions (Hilton et al., 2021; Horan et al., 2019). Analyses of solid samples in near-surface weathering profiles of black shales has found that the pattern of Re depletion as a function of decreasing depth matches the pattern in OC_{petro} depletion (Jaffe et al., 2002; Peucker-Ehrenbrink and Hannigan, 2000). Measurements of weathered materials from bedrock with lower OC_{petro} content in Taiwan and New Zealand have also observed a coincidence in the zones of depletion of Re and OC_{petro} (Hilton et al., 2014; Horan et al., 2017).

There is limited information about potential biologic Re cycling. Dolor et al. (2009) conclude that in a bacterial culture including four strains of anaerobic bacteria commonly found in marine and estuarine sediments that they did not remove significant amounts of perrhenate from the aqueous phase during growth at neutral pH. However, in the Chilika Lagoon, Danish et al. (2021) conclude that some coastal macroalgae and macrophytes might uptake Re during their biological activities. This observation is supported by previous work by some for Re uptake by brown algae in seawater (Kučera et al., 2006; Yang, 1991).

One way to evaluate the association of Re release with either OC_{petro} or sulfides is to examine the concentration-runoff (C-R) relationship of the dissolved chemical load of rivers. Concentration-runoff relationships can reflect the integration of multiple upstream hydrogeochemical processes, thus they are useful in analyses of solute origin and fate at large spatial scales that control runoff chemistry (Aguilera and Melack, 2018; Godsey et al., 2009; Maher, 2011). Concentration-runoff relationships are often linear on logarithmic axes, which indicates there is a power-law relationship (Eq. (1)) between concentration and instantaneous runoff (Godsey et al., 2009),

$$C = a \times R^b \quad (1)$$

where C is the concentration, R is the runoff, a is a constant that is a function of solute and catchment characteristics, and b is the dimensionless power rate exponent indicating the slope of the relationship. These power law equations are sometimes represented as a function of discharge (Q); however, we use the parameter of runoff, which is discharge normalized by basin area. The variable of

runoff allows for easier comparison of behavior in watersheds of different sizes.

In addition to the slope, solute hysteresis (both presence/absence and rotational direction) across a range of runoff conditions can be used to infer dominant flow pathways and dominant solute sources (Evans and Davies, 1998). When solute concentrations in a catchment are relatively stable over a wide range of flows, the C-R pattern is relatively "chemostatic", as is often observed during the weathering of bedrock-derived solutes (Ameli et al., 2017; Hoagland et al., 2017; Thompson et al., 2011). When the concentration changes with changing flow, the C-R pattern is more "chemodynamic", reflecting either the activation of additional solute sources (positive C-R slope) or source-limitation (negative C-R slope). For example, more steeply negative C-R relationships that have been observed for SO_4^{2-} are thought to reflect deep weathering fronts of sulfide minerals and therefore source limitation occurring at high flow when flowpaths above the depletion front become more dominant (Gu et al., 2020a; Gu et al., 2020b; Kanzaki et al., 2020). By examining the C-R relationships of Re relative to other solutes, it is possible to gain insight regarding reactions along flow pathways, depth of flowpath, near stream or riparian processes, and in larger rivers, mixing of heterogeneous tributaries (Godsey et al., 2009; Kim et al., 2017; Knapp et al., 2020; Maher and Chamberlain, 2014; Musolff et al., 2015; Rose et al., 2018).

Here we examine the C-R patterns of dissolved solutes in two small mountainous rivers: the Eel and Umpqua Rivers in the Pacific Northwest, USA. The Eel and Umpqua Rivers share many key characteristics in terms of size, runoff, climate, and vegetation, but they have a roughly 15-fold difference in sediment yield and erosion rate due to their tectonic setting. The C-R patterns of Re are compared to those of other dissolved solutes, including major cations and anions, trace elements, nutrients, and $^{87}Sr/^{86}Sr$ isotope ratios. In addition to examining concentrations over a wide range of runoff conditions, we also examined solute behavior during individual storm events and quantified the coefficient of variation of concentration relative to the coefficient of variation of runoff in order to better constrain the sources and processes affecting riverine dissolved Re. Using the range in erosion rates among the individual catchments, we also evaluated the role of erosion in controlling Re supply.

2. Methods

2.1. Site information

The Pacific Northwest coast of the United States is lined with many small mountainous rivers (10^2–10^4 km^2 drainage area) that contribute significantly to freshwater runoff and transport of dissolved fluxes into the ocean from land during winter storms (Goñi et al., 2013; Wheatcroft and Sommerfield, 2005). Given the regional and also global importance of small mountainous rivers (Milliman and Farnsworth, 2013), we chose to investigate the Umpqua and Eel Rivers, which share many key characteristics (Table 1, Fig. 1) but also display several differences.

The Umpqua River drains the Oregon Coast Range, the Western Cascade and High Cascade Mountains, and the northern portion of the Klamath Mountains (Ramp, 1972). The geology of the Coast Range province within the Umpqua River basin is predominantly Eocene sandstone, siltstone, and mudstone rocks. The Cascades are comprised of andesitic and basaltic volcanic rocks, ranging in age from late Eocene through Late Miocene in the Western Cascades to Pliocene and Pleistocene in the High Cascades. The Klamath mountains in the southern part of the Umpqua basin include Mesozoic sandstone, conglomerate, and greywacke, metamorphosed mudstone, siltstone, and greywacke, as well as lesser amounts of metamorphosed volcanic rocks and serpentinites.

Table 1
Summary of River and Watershed Characteristics.

Variable	Umpqua	Eel
Basin Characteristics		
Total Basin Size (km^2)	13,000	9537
Length of main channel (km)	179	193
Maximum elevation (m)	2799 (Mt. Thielsen)	2311 (Solomon Peak)
Geologic provinces	Oregon Coast Range, Cascades, and Klamath Mountains	Coastal Belt Franciscan and Central Belt Franciscan
Predominant Basin Geology	Cenozoic volcanic rocks, Cenozoic sedimentary rocks	Cenozoic and Mesozoic sedimentary rocks
Basin Vegetation	Douglas-fir forests, mixed conifer/hardwood forests	Mixed Douglas-fir and hardwood forests, Redwood forests, oak woodlands, grasslands[a]
Major Land Use	Forestry, grazing, recreation	Forestry, grazing, recreation
Climate	warm, dry summers and cool, wet winters	warm, dry summers and cool, wet winters
Annual Precipitation (mm)	800–>2500 (basin mean = 1310)[b]	1000–2000 (basin mean = 1560)[b]
Annual Temperature Averages (°C)	T_{min} = −1 to 8 T_{max} = 13–18	T_{min} = 3–11 T_{max} = 17–23
Above ground biomass (kg C m^{-2})	14 (living), 3 (dead)[c]	14 (living), 2 (dead)[c]
Net primary productivity (kg C m^{-2} yr^{-1})	0.6	0.6
Soil Carbon inventories (kg C m^{-2})	12[c]	5[c]
USGS Gauging Station	Elkton (USGS ID: 14321000, 43.586N, 123,554W)	Scotia (USGS ID:11477000, 40.492N, 124.099W)
Hydrologic Characteristics		
Drainage area (km^2)	9539 (73% of total basin)	8063 (85% of total basin)
Average basin slope (degrees)	17.6	18.4
Daily discharge (Avg ± s.d.) (m^3 s^{-1})	208 ± 305	208 ± 517
Annual runoff (Avg) (mm yr^{-1})	819	692
Specific water yield (mm)	692	819
Average annual sediment load ($\times 10^9$ kg)	1.4[d]	18[d]
Sediment yield ($\times$tons km^{-2} yr^{-1})	147	2232

[a] Omernik (1987).
[b] USGS StreamStats.
[c] Goñi et al. (2013).
[d] Wheatcroft and Sommerfield (2005).

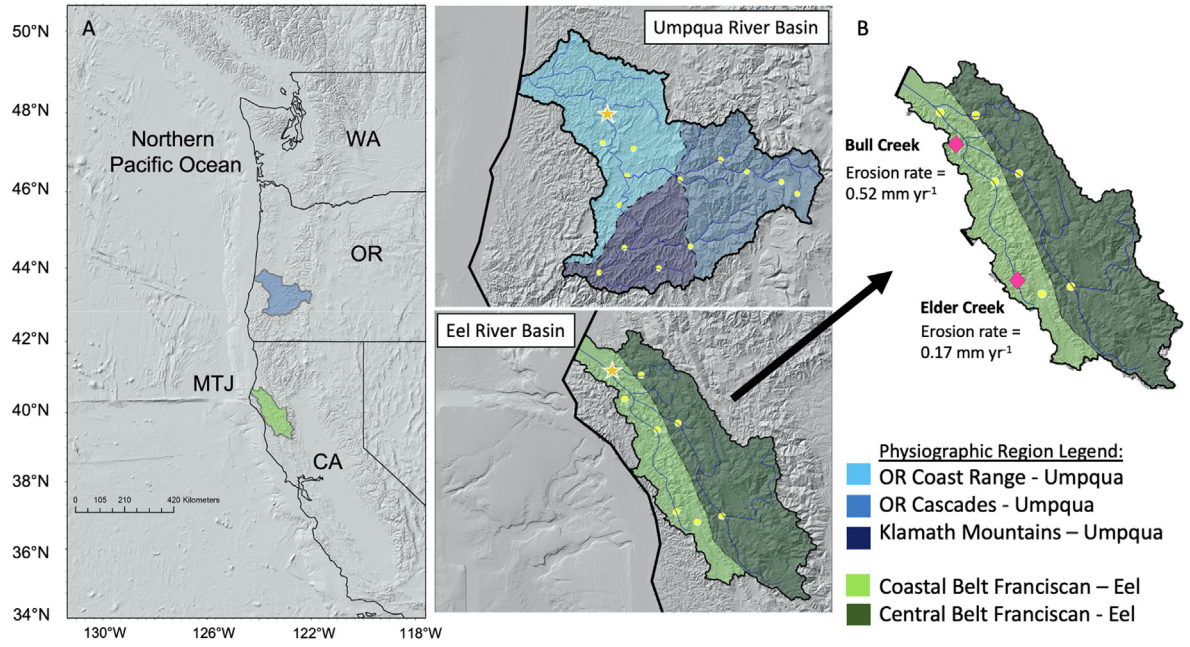

Fig. 1. (a) Physiographic regional map of the Umpqua and Eel watersheds. The location of the USGS gauging stations sampled is shown in yellow circles, and the farthest downstream sampled USGS stations in the Eel and Umpqua are marked with yellow stars. The regional map shows the locations of the two watersheds relative to the Mendocino Triple Junction (MTJ), Washington, Oregon, and California. The physiographic regions of the Umpqua watershed (13,000 km^2) are the Oregon Coast Range, the Oregon Cascades (including High and Western), and the Klamath Mountains. The physiographic regions of the Eel watershed (9537 km^2) are the Coastal Belt Franciscan and the Central Belt Franciscan. (b) Eel River map highlighting the location of Bull Creek and Elder Creek with pink diamonds. Erosion rates are reported from Willenbring et al. 2013. (For interpretation of the references to colour in this figure legend, the reader is referred to the web version of this article.)

The Eel River drains the California Coastal Range with extensively sheared and fractured rocks, namely Coastal Belt Franciscan Complex and the Central Belt Franciscan Complex. The Franciscan complex is heterogeneous in its make up, but its lithologies are dominated by clastic sedimentary rocks, including greywacke sandstones, schist, limestone, and conglomerates, which have experienced some low-grade metamorphism (Ernst, 2011). Most of the Coastal Belt Franciscan within the Eel River tributaries studied here is Yager terrane, an Eocene age assemblage of arkosic sandstone and argillite (Langenheim et al., 2013). The basin geology of Eel River tributaries in the Central Belt Franciscan is known to have higher rock strength and is more prone to landsliding and earthflows (Brown and Ritter, 1971; Mackey and Roering, 2011). The Central Belt consists predominantly of Franciscan argillitic mélange including large blocks of sandstone, shale, and occasional meta-basalt and meta-sandstone (Bennett et al., 2016; Langenheim et al., 2013). Organic matter in the Central Belt is more thermally mature than organic matter in the Coastal Belt as characterized by vitrinite reflectance (Underwood et al., 1988). It is unclear how previous events of metamorphism might alter Re concentrations and release. While there is limited solid phase data throughout either the Umpqua or the Eel, there is some evidence of petrogenic organic carbon respiration at a weathering profile near Elder Creek, measured through radiocarbon of CO_2 gas (Tune 2021). Characterization of the particulate matter of these two rivers is reported in previous studies (Goñi et al., 2013; Hatten et al., 2012; Wheatcroft et al., 2010). Overall, POM in the Umpqua is characterized by a mostly biogenic load in all measured discharges with only ~5% OC_{petro} in the suspended load. In the Eel, there are enhanced contributions of mineral sediment that occur during both high and low flows with roughly 50% OC_{petro} and roughly 50% aged biogenic OM in the suspended load (Goñi et al., 2013).

The Eel River has the highest known sediment yield in the contiguous US due to the friable nature of its lithology and tectonic setting (Blair et al., 2003; Willenbring et al., 2013). The Eel watershed is located near the Mendocino Triple Junction and has higher tectonic uplift rates than the Umpqua watershed to the north (Goñi et al., 2013; Langenheim et al., 2013; Lock et al., 2006) (Fig. 1). The long-term (1950–1990) sediment yield from Eel basin (2232 tons km^{-2} yr^{-1}) is over 15 times greater than that of the Umpqua (147 tons km^{-2} yr^{-1}) (Goñi et al., 2013). Erosion rates in the Eel River basin and the Umpqua River at Elkton were previously determined using ^{10}Be data (Table 2, Balco et al., 2013; Fuller et al., 2009; Willenbring et al., 2013). In addition, suspended sediment yield data are available for multiple specific tributaries of the Umpqua River (Curtiss, 1975; Karlin, 1980; Wise and O'Connor, 2016) (Appendix A Table S1).

The Eel and the Umpqua basins have a climate that consists of warm, dry summers and cool, wet winters. Most precipitation occurs between October and April. Annual precipitation is similar between the two basins, where the Umpqua ranges between 800 and >2500 mm (basin mean 1310 mm) and the Eel ranges between 1000 and 2000 mm (basin mean 1560 mm). Annual runoff is 692 mm in the Umpqua basin and 819 mm in the Eel basin (Table 1). Both rivers transport the majority of their materials and water fluxes (>80%) during high discharge, winter storm events (Goñi et al., 2013). Both watersheds are predominantly forested, with land use that includes commercial forestry, cattle grazing, and dispersed rural development.

Elkton (USGS Site: 14321000) and Scotia (USGS Site: 11477000) are the furthest downstream USGS gauged sites on the Umpqua and Eel rivers without tidal influence. These two sites (Elkton and Scotia) are used to represent the data presented as "Umpqua" or "Eel", respectively, as they integrate the waters of the upstream tributaries that are nested within those larger watersheds. The one exception is the Eel River tributary the Van Duzen River, which joins the main stem of the Eel just downstream of Scotia. All sampled tributaries of the Eel (n = 9) and Umpqua (n = 12) are listed in Table 2. An extended version of Table 2 is available in Appendix A as Supplementary Table 1.

2.2. Collection of water samples

River samples were collected in October 2015, November 2017, December 2017, March 2018, January 2019, February 2019, and

Table 2
USGS Data Site Information Summary.

Watershed	USGS Gauge Site	n samples	Sampling Dates	Drainage Area (km^2)	Geology
Cahto Creek	11475610	3	2017, 2018, 2019	13	Coastal Belt Franciscan
Elder Creek	11475560	16	2017, 2018, 2019	17	Coastal Belt Franciscan
South Fork at Leggett	11475800	3	2015, 2017, 2018	642	Coastal Belt Franciscan
Miranda	11476500	3	2015, 2017, 2019	1391	Coastal Belt Franciscan
Bull Creek	11476600	23	2017, 2018, 2019	73	Coastal Belt Franciscan
Van Duzen	11478500	17	2015, 2017, 2018, 2019	575	Central Belt Franciscan
Ft. Seward	11475000	2	2015, 2017	5457	Central Belt Franciscan
Dos Rios	11473900	4	2015, 2017, 2018, 2019	1930	Central Belt Franciscan
Eel at Scotia	11477000	14	2015, 2017, 2018, 2019	8063	Mixed Central Belt and Coastal Belt Franciscan
Clear Water River above Trap Creek	14314500	1	2017	108	Oregon Cascades
Steamboat Creek near Glide	14316700	2	2015, 2017	588	Oregon Cascades
Little River at Peel	14318000	1	2017	458	Oregon Cascades
North Umpqua above Copeland Creek	14316500	2	2015, 2017	1230	Oregon Cascades
Cow Creek near Azalea	14309000	1	2017	202	Klamath Mountains
West Fork Cow Creek near Glendale	14309500	2	2017, 2019	225	Klamath Mountains
Cow Creek near Riddle	14310000	3	2015, 2017, 2019	1181	Klamath Mountains
Little Wolf Creek	14320934	15	2017, 2019	23	Oregon Coast Range
Lookingglass Creek at Brockway	14311500	1	2017	409	Oregon Coast Range
Calapooya Creek near Oakland	14320700	2	2017, 2019	544	Oregon Coast Range
South Umpqua at Tiller	14308000	1	2017	1163	Mixed Oregon Coast Range and Oregon Cascades
North Umpqua at Winchester	14319500	2	2015, 2017	3481	Mixed Oregon Coast Range and Oregon Cascades
Umpqua at Elkton	14321000	11	2015, 2017, 2019	9539	Mixed Oregon Coast Range and Oregon Cascades

Additional information is shown in Appendix A Table S1.

April 2019. These sampling times capture periods of a range of precipitation and discharge, including end-of-summer low flow, winter elevated baseflow, and some storm events (Fig. 2 and Appendix A Table S2). Water sampling was done manually with clean bottles or buckets from the middle of the channel, or by using ISCO samplers collecting at four-hour intervals in the case of Elder Creek, Bull Creek, Van Duzen, and Little Wolf Creek storm events. For all grab samples, temperature and pH were measured in the field during collection.

Precipitation samples were also collected using the method outlined in Hynicka et al. (2016). Acid washed 1.0 L LDPE bottles equipped with acid washed 16 cm diameter polypropylene funnels and 2 mm polypropylene screen mesh were placed 1 m above ground in clearings from Ten Mile in the Umpqua Basin and the Angelo Coast Reserve near Elder Creek in the Eel Basin. Precipitation samples were then acidified with 1% with ultrapure HNO_3, and refrigerated.

2.3. Water chemistry analysis

Streamwater samples were filtered using 0.2 μm and 0.8 μm polyethersulfone (PES) filters, either immediately upon sampling or within 24 h using pre-cleaned filter units. The 0.8 μm PES filters were used for all sampling trips; however, both 0.2 μm and 0.8 μm PES filters were used in parallel for samples from the November 2017, December 2017, and March 2018 sampling campaigns. The purpose of collecting water samples with both the 0.2 μm and 0.8 μm filters in parallel was to assess the potential importance of colloids in the 0.2 μm to 0.8 μm size range on solute chemistry. All data used in the subsequent discussion of C-R analyses are from samples that were filtered using a 0.8 μm filter. When discussing colloids specifically, however, we address the comparison between the 0.2 μm and 0.8 μm filtered samples. All water samples intended for cation and Re analysis were acidified in the field to pH ~ 2 and stored in acid-cleaned LDPE bottles.

For all grab samples, a separate aliquot of the filtered sample was collected in 350 mL amber glass bottles with crimp-sealed polyurethane lined metal caps, preserved with ~30 μmol $HgCl_2$ for TCO_2 and pCO_2 analysis. The TCO_2 and pCO_2 analyses were made following methods described in Bandstra et al. (2006). Briefly, the system is based on a gas-permeable membrane contactor that draws a sample at a continuous flow rate. The sample is acidified in a mixing coil with 10% HCl supplied by a peristaltic pump, and the liquid flows inside of the tubing. Counter to the liquid, a CO_2-free gas stream strips evolved CO_2 from the solution. This gas stream is dried with dry air across a membrane until it is detected by a nondispersive infrared sensor, which measures the mole fraction of CO_2. The TCO_2 and pCO_2 parameters were then used to solve for the other carbonate system parameters via a simple mass balance.

Samples for anions analyses were not acidified and were stored in separate clean LDPE bottles that were not acid-washed. Concentrations of anions (Cl, NO_3^-, PO_4^{3-}, F^- and SO_4^{2-}) were determined using a Dionex 1500 Ion Chromatograph using the US EPA Method 9056A at the Cooperative Chemical Analytical Laboratory at Oregon State University.

2.3.1. ICP-MS

Dissolved Mo, Re, and U concentrations of filtered and acidified river water samples were analyzed using an isotope dilution method. Samples were spiked in Teflon vials. All samples from the Eel River were spiked with 200 μl of spike blend (containing ^{100}Mo, ^{135}Ba ^{185}Re, and ^{236}U) per 10 mL of sample, and all samples from the Umpqua River were spiked with 100 μl of spike blend per 10 mL of sample. Samples were evaporated to near dryness, and then 2 mL of 3% HNO_3 was added to the samples for analysis. Samples were analyzed with a Thermo Scientific X-Series II quadrupole ICP-MS at the Keck Collaboratory at Oregon State University. The minimum detection limit was determined using the standard deviation of the abundance ratio determined from previous abundance data for the spike (Yu et al., 2002). The minimum limit of detection for Re was 0.0355 ppt. Thulium and Yb oxide production were monitored and found to contribute less that 0.4% and 0.05%, respectively, to masses 185 and 187. Accuracy and precision of the measurements of Re, Mo, and U were determined with external standard Canadian River water standard SLRS-5. Analysis of $[Re]_{diss}$ in SLRS-5 produced a value of 61.9 ± 2.5 ppt (n = 25, ±2σ) in

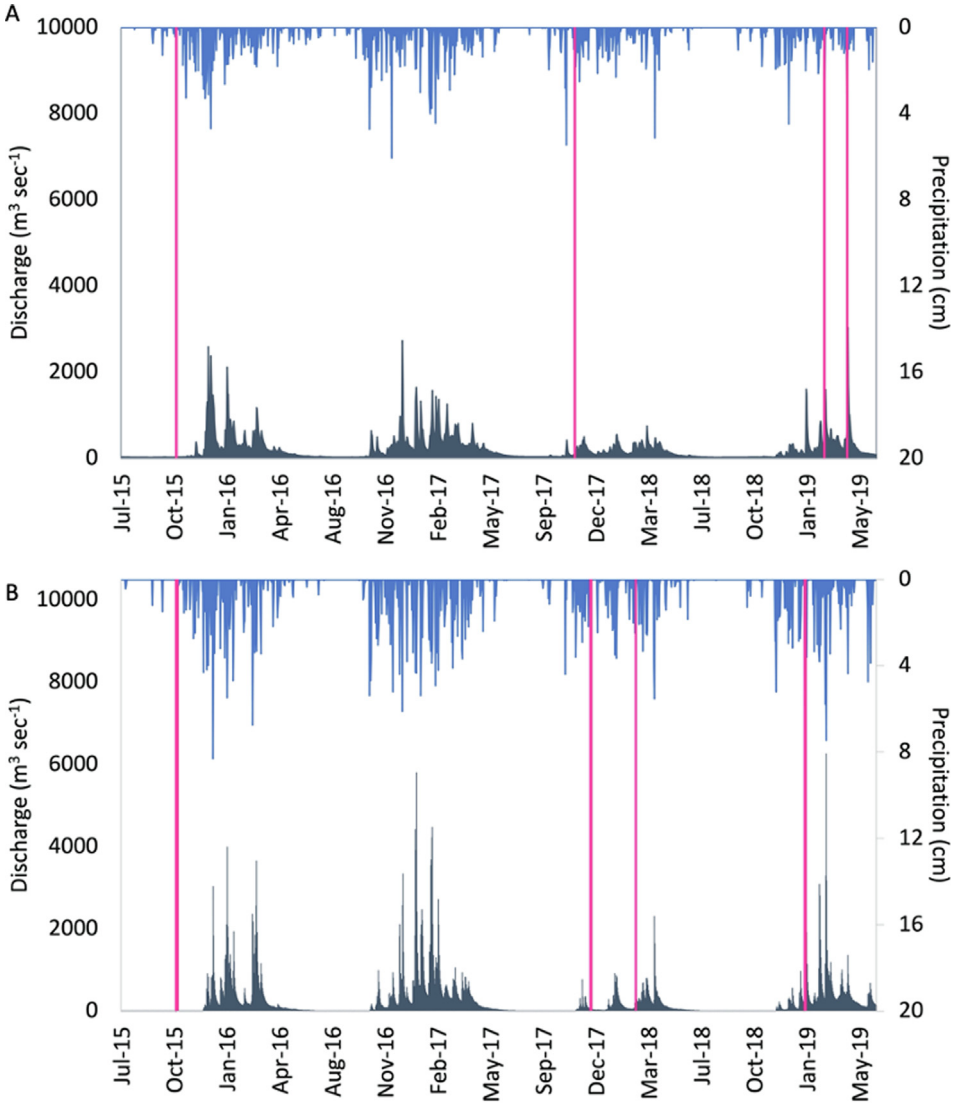

Fig. 2. (a) Discharge rates and daily precipitation amounts for the Umpqua River based on data from USGS Gauging Site Elkton (USGS ID: 14321000). Light pink lines denote dates of sampling campaigns. (b) Discharge rates and daily precipitation amounts for the Eel River based on data from USGS Gauging Site Scotia (USGS ID: 11477000). Light pink lines denote dates of sampling campaigns. (For interpretation of the references to colour in this figure legend, the reader is referred to the web version of this article.)

agreement with previously reported values of 66 ± 12 ppt (Yeghicheyan et al., 2013) and 59.8 ± 1.7 ppt (Horan et al., 2019).

2.3.2. ICP-OES

Major cations were measured with a Spectros Arcos ICP-OES in axial mode at the Keck Collaboratory at Oregon State University. Dissolved cations analyzed include: Al, B, Ba, Ca, Fe, K, Li, Na, Mg, S, Si, and Sr. Concentrations were determined using a multi-element external calibration standard prepared at 5 different concentrations to mimic natural river water concentrations. Accuracy and precision of the ICP-OES measurements was determined using external standard Canadian river water certified reference material SLRS-6 and SLRS-5. Measured values were within 10% of reported values for Na and K and within 5% for all other elements.

2.3.3. MC-ICP-MS

For Sr isotopic analysis, an aliquot of the filtered and acidified river samples containing ~30 ng of Sr was purified using 50 µl of Eichrom Sr-Spec resin. Isotopic measurements were made on a Nu Plasma© multi-collector ICP-MS at the W. M. Keck Collaboratory for Mass Spectrometry at Oregon State University, and on a Nu Plasma© multi-collector ICP-MS at the University of Texas El Paso. Masses 83–88 were monitored in static collection mode. Masses 83 and 85 were monitored for Kr (blank only) and Rb (standards and samples) interferences, respectively. Strontium isotope ratios were measured 40 times per sample. Reported values are corrected to $^{86}Sr/^{88}Sr$ = 0.1194 and Sr standard NBS-987 $^{87}Sr/^{86}Sr$ = 0.710245. For samples analyzed at Oregon State University, the external reproducibility and the experimental precision reported for our Sr-isotope data are based on in-house standard EMD (n = 15) with an average value of 0.70818, 2σ = 0.000035. For samples analyzed at University of Texas El Paso, the external reproducibility and the experimental precision reported for our Sr-isotope data are based on analyses of BCR-2 (n = 8) with an average value of 0.70501, in agreement with previously reported values, with a 2σ = 0.000015.

2.4. Data analysis

The charge balance of major dissolved cations (Total $Z^+ = 2Ca^{2+} + K^+ + 2\,Mg^{2+} + Na^+$) and dissolved anions (Total $Z^- = Cl^- + HCO_3^- + 2SO_4^{2-}$) was determined using Eq. (2) as a measure of data quality.

$$([TZ^+ - TZ^-]/[TZ^+ + TZ^-]) \quad (2)$$

The average charge balance was 3% (±5% 1S.D.) across all samples.

In order to analyze stream water fluxes derived from weathering, the atmospheric input contribution was subtracted from the stream water chemistry. Atmospheric input corrections were made for Ca^{2+}, K^+, Mg^{2+}, Na^+, and SO_4^{2-} only. Stream water chloride concentrations were used to make these corrections, using.

$$[X]^* = [X] - (X/Cl)_{rain} \times [Cl]$$

where [X]* denotes the stream concentration in molar units corrected for atmospheric inputs, [X] denotes the measured stream concentration in molar units, $(X/Cl)_{rain}$ is the measured long-term mean annual molar ratio of atmospheric inputs, and Cl is the measured stream Cl^- concentration. Molar ratios for atmospheric inputs were derived from rainfall chemistry measurements from the National Trends Network of the National Atmospheric Deposition Program (NADP). The atmospheric correction for the Eel River was based on a combination of precipitation chemistry measured in the Elder Creek watershed by Kim et al. (2014) and on precipitation chemistry of Hopland, CA (Site ID: CA45). We observed a minor difference between the corrections for Ca^{2+*}, Mg^{2+*}, and Na^{+*} using the molar ratios from Kim et al. (2014) or Hopland; however, the molar ratio of K^{+*} measured by Kim et al. (2014) is about 4.5x as great as the molar ratio of K^+/Cl^- at Hopland and in seawater. Therefore, the atmospheric correction for K^{+*} was based on the molar ratio measured at Hopland. There was no SO_4^{2-}/Cl^- molar ratio data collected by Kim et al. (2014), thus molar ratio used for SO_4^{2-} is derived from Hopland. The atmospheric correction for the Umpqua River was based on precipitation chemistry of Alsea, OR (Site ID: OR02). The rainwater chemistry data collected at Alsea and Hopland was using wet-only precipitation data, while the rainwater chemistry data collected at Elder Creek was collected using openfall precipitation data. The choice of atmospheric correction made little difference for the observed pattern with runoff. In the Eel, the average atmospheric correction was 2% for Ca^{2+}, 16% for K^+, 7% for Mg^{2+}, 40% for Na^+, and 26% for SO_4^{2-}. In the Umpqua, the average correction was 2% for Ca^{2+}, 10% for K^+, 7% for Mg^{2+}, 39% for Na^+, and 26% for SO_4^{2-}. Other chemical species, such as Re, Al, B, Ba, Br, Cl^-, Fe, Li, Mo, NO_3^-, PO_4^{3-}, Si, Sr, and U were not corrected for atmospheric inputs.

For the C-R relationships, the intercepts (a-values) and slopes (b-values) were calculated using RStudio package (R Core Team (2020); https://www.R-project.org/) via power law regression function. A slope of zero indicates that the system maintains constant river solute concentrations across a wide range of runoff. A positive slope of >0 describes mobilization behavior with increasing runoff. At the opposite end of the spectrum, a slope of −1 indicates pure dilution of solute concentrations with increasing runoff. A simple estimate of concentration at mean runoff was made using the calculated power law relationship and the mean runoff based on USGS long-term discharge data for water years 2015–2019. These concentrations are reported in Appendix A Table S3. The p-values and the 95% confidence interval of the intercepts and slopes of the C-R relationship were also calculated using RStudio stats package (R Core Team (2020); https://www.R-project.org/) via power law regression function. We also calculated the ratio of the coefficient of variation of the concentration to the coefficient of variation of the runoff (CV_C/CV_R) which provides another framework for evaluating C-R relationships. This is especially useful when the slope (b value) of the C-R power law is approximately 0 (Thompson et al., 2011), because it can distinguish variability or invariance within the general slope of the C-R relationship. Low concentration variability behavior is represented by CV_C/CV_R < 0.5, meanwhile CV_C/CV_R > 1 is indicative of high concentration variability behavior (Musolff et al., 2015). The term "chemostatic" applies to solutes with a b-value near 0 and a CV_C/CV_R < 0.5, while the term "chemodynamic" can be used for all other cases. In Table S4, we report three categories of p-values for the C-R relationships of tributaries. A p-value<0.001 is denoted with an A; a p-value <0.05 is denoted with a B; and a p-value>0.05 is denoted with a C. Statistically, a p-value >0.05 is considered to be not significant, but we report all three designated categories of p-values in Table S4 to provide a further level of detail to the C-R relationship and CV_C/CV_R of different elements. All C-R relationship parameters are reported in Appendix A Table S4.

3. Results

The range of runoff sampled for the Eel River in this study spans over 3 orders of magnitude from 0.01 mm day^{-1} during summer low flow to 22.54 mm day^{-1} during winter storm conditions (Hydroshare data). For comparison, USGS historical data (1988–2019) for the Eel at Scotia has a total range of 0.01 mm day^{-1} to 109.2 mm day^{-1}. For the Umpqua, the range of runoff captured in our sampling spans 2 orders of magnitude from 0.26 mm day^{-1} during summer low flow, to 27.01 mm day^{-1} during winter storm conditions. USGS historical discharge data (1988–2019) for the Umpqua at Elkton has a total range of 0.2 mm day^{-1} to 43.6 mm day^{-1}. Due to changes in USGS stream monitoring, some tributaries did not have data for certain dates. In this case, daily discharge was extrapolated using a linear regression between historical USGS data at the site missing water data and a USGS data at a nearby site with similar hydrologic behavior. In the Eel River basin, Bull Creek discharge data in 2019 was calculated based on USGS Site 11469000 Mattole River Near Petrolia, CA. Cahto Creek mean annual runoff was extrapolated from USGS site 11475800 South Fork Eel at Leggett. In the Umpqua River basin, Calapooya Creek and Lookingglass Creek were extrapolated from USGS Site USGS 14312000 South Umpqua River Near Brockway, OR.

We compared the data collected for this study to available longer term data for major cations and anions in these watersheds (Appendix A Fig. S1). Data across low and high discharges were similar to previous measurements by the USGS and also Oregon Department of Environmental Quality (DEQ), with the exception of a deviation in the data we collected at Elkton at high runoff (Appendix A Fig. S1f). We utilized dissolved $^{87}Sr/^{86}Sr$ ratios of stream water to determine the contribution of different tributaries in the Umpqua and Eel watersheds. Within the Umpqua, tributaries draining the volcanic western Cascades have much lower $^{87}Sr/^{86}Sr$ ratios (<0.704), relative to the rest of the Umpqua basin (0.705–0.708). The dissolved $^{87}Sr/^{86}Sr$ ratios indicate that this deviation at Elkton is likely due to the fact that our high flow sampling occurring during storm events in February and April of 2019 that were centered on the western Coast Range side of the Umpqua basin, whereas the USGS and DEQ data represent water data compiled over decades, averaging across many events covering the whole Umpqua basin. (see discussion in Appendix A and Figs. S2 and S3).

3.1. Solute chemistry

3.1.1. Broad comparison of the Eel and Umpqua

Bicarbonate dominates dissolved anions in both river basins, followed by Cl^- and SO_4^{2-*} (Fig. 3 and Appendix A Table S3). In the Eel River, the Na^{+*}concentration was 1.2 times higher, Ca^{2+*} was 2.8 times higher, and Mg^{2+*} was 2.4 times higher as compared to the Umpqua. The dissolved Re concentration at mean runoff in the Eel River is 2.4 times higher, at 3.54 pmol/L, as compared to 1.48 pmol/L in the Umpqua River. The SO_4^{2-*} concentration at mean

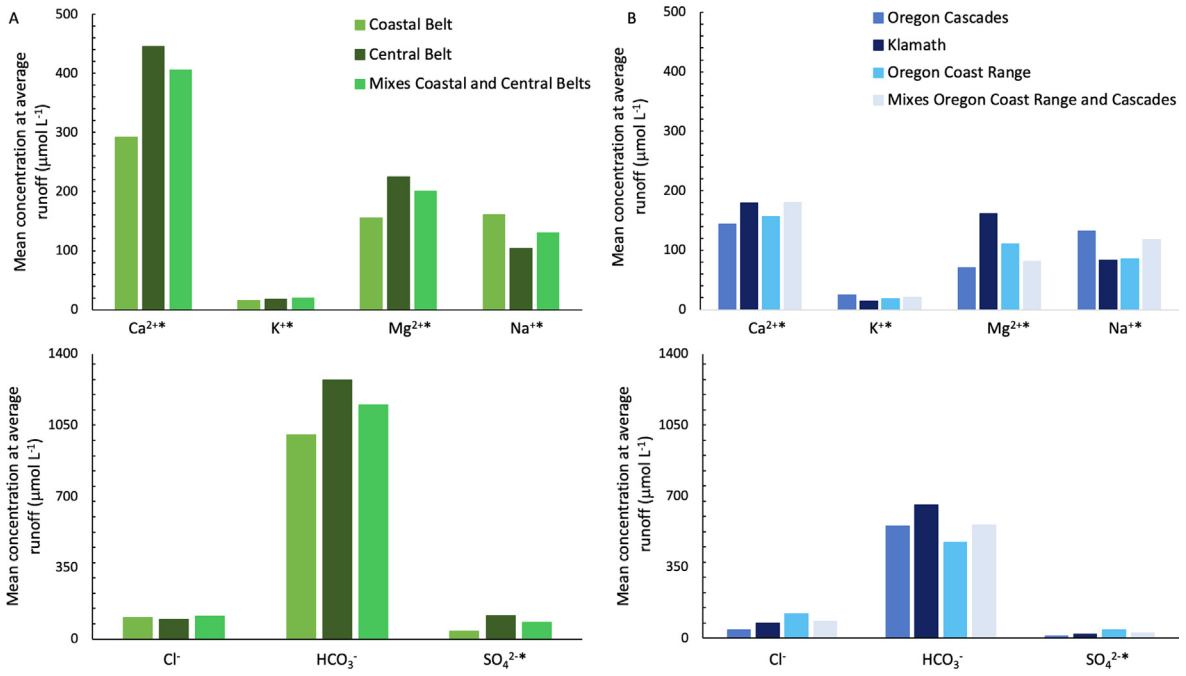

Fig. 3. Comparison of mean concentration of major cations and anions at average runoff for USGS water years 2015–2019 by physiographic region in the Eel (A) and Umpqua (B) Rivers.

runoff in the Eel River is 4.0 times higher than in the Umpqua River, and the HCO_3^- concentration at mean runoff is 2.5 times higher in the Eel River than the Umpqua River. The concentration of Al is 1.1 times higher in the Eel compared to the Umpqua, and the concentrations of Mo and U are 4.3 and 4 times greater than in the Umpqua. Strontium concentrations are 3.8 times higher in the Eel River. In contrast, the SiO_2 concentration at mean runoff was 1.8 times higher in the Umpqua River. The concentrations of Fe and K^{+*} are 1.1 times greater in the Umpqua compared to the Eel River, and the concentrations of nutrients, such as NO_3^- and PO_4^{3-}, are 2 and 1.4 times greater, respectively, in the Umpqua basin than in the Eel (Appendix A Table S3).

3.1.2. Umpqua River tributaries

Tributaries within the Umpqua Basin are discussed based on their location with respect to three physiographic regions: the Cascades with volcanic lithology (including both the High Cascades and Western Cascades), the Klamath Mountains with both sedimentary and metamorphic lithology, and the Oregon Coast Range with sandstone and siltstone sedimentary lithology. Tributaries across all three physiographic regions have similar Ca^{2+*}, Mg^{2+*}, and Na^{+*}. Solute concentrations of SiO_2 were generally higher in the Cascade tributaries, while SO_4^{2-*} and Re concentrations were generally lower in the Cascades than in other parts of the watershed. Rhenium concentrations at mean runoff were highest in the Coast Range and Klamath draining tributaries and lowest in the volcanic underlain Cascades (Appendix A Table S3). Concentrations of Al, Fe, NO_3^- and U were greatest in tributaries in the Coast Range, while concentrations of K^{+*}, Mo, and PO_4^{3-} were greatest in the Cascades. Mean HCO_3^- and Sr concentrations were highest in the Klamath tributaries.

3.1.3. Eel River tributaries

Tributaries of the Eel Basin are grouped into two physiographic regions: the Coastal Belt Franciscan and the Central Belt Franciscan. Concentrations of SO_4^{2-*} are lower in tributaries draining in the Coastal Belt compared to tributaries draining Central Belt with the exception of the northern Coastal sites of Miranda and Bull Creek. Mean Re concentrations in tributaries draining Coastal Belt Franciscan and Central Belt Franciscan were similar. Silica concentrations were slightly higher in the Coastal Belt Franciscan (Appendix A Table S3). Concentrations of Al, Fe, HCO_3^-, NO_3^-, Sr and U were greater in the Central Belt Franciscan. Phosphate mean concentration was slightly greater in the Coastal Belt Franciscan. The concentration of K^{+*} and Mo were similar in tributaries draining in the Central Belt and Coastal Belt.

3.2. Solute concentration-runoff (C-R) patterns

Calculated b-values of the C-R relationship based on data collected in this study (labelled "OSU"), as well as for the previously collected USGS or DEQ data where available are presented in Table S4. For a majority of the solutes reported from this study and from historical USGS and DEQ water chemistry data, logarithmic C-R relationships of atmospheric corrected data appear to be linear (Appendix A Fig. S1), which suggests that a simple power law may be used to evaluate the relationship of concentration and runoff at these sampling stations. In contrast, visual inspection of C-R relationships showed that historical USGS water chemistry SO_4^{2-*} data at two sites, Scotia and Elder Creek, did not show a single pattern, but instead a 2-part pattern with relatively constant concentration at low runoff and decreasing concentrations at higher runoff (Appendix A Fig. S1a and Fig. S1c). For these SO_4^{2-*} data, separate C-R relationships were determined by bifurcating the data to below and above mean runoff (Fig. 7 and Appendix A Figs S4, S5, and S6).

Comparison of this study's calculated C-R relationships to those based on the USGS data of the Eel River at Scotia yields power law exponents that are consistent within the uncertainty of the relationship for all dissolved solutes (Appendix A Table S4). Comparison of this study's calculated C-R relationships to the USGS data of the Umpqua River at Elkton yields power law exponents that are consistent within the uncertainty of the relationship for SiO_2 (Appendix A Table S4). However, there are differences in the b-

values, as well as larger uncertainties for Ca^{2+*}, Mg^{2+*}, SO_4^{2-*}, HCO_3^- calculated from this study and from previously available USGS data for Umpqua River at Elkton. We attribute this to the effect of our sampling of storm events which were centered only on the western side of the basin, as described earlier (see discussion in Appendix A).

3.2.1. C-R patterns of major cations and anions

Solutes such as Ca^{2+*}, Mg^{2+*}, Na^{2+*}, and HCO_3^- have negative calculated b-values and, most of the time, $CV_C/CV_R < 0.5$. Rhenium b-values tended to be in the same range as those of other major cations (Ca^{2+*}, Mg^{2+*}, and Na^{+*}) and HCO_3^-, while SiO_2 was nearly chemostatic. Concentration-runoff relationship of SiO_2 have b-values closest to zero and $CV_C/CV_R < 0.5$. In both the Eel and Umpqua Rivers, the b-value for silica was most chemostatic (b = ~0), relative to other elements. In the Eel, the Re b-value is −0.14, which was similar to that of Ca^{2+*} (b = −0.15), Mg^{2+*} (b = −0.17), and Na^{+*} (b = −0.13). In the Umpqua, the Re b-value is −0.09, which is similar to the b-value for Ca^{2+*} (b = -0.14), Mg^{2+*} (b = −0.16) and Na^{+*} (b = −0.10) (Appendix A Table S4).

Sulfate had the most negative b-value in both the Eel and Umpqua (b = −0.21 and b = −0.31, OSU data respectively). While the uncertainties of Re and SO_4^{*2-} overlap in many cases, the calculated b-value of SO_4^{*2-} is more negative than that of Re at all six of the tributaries with statistically significant (p value < 0.05) C-R relationships (Fig. 4 and Appendix A Table S5). In the instance of Elder Creek, Bull Creek, and Van Duzen, the b-value of SO_4^{2-*} is about twice as negative as the b-value of Re. At most locations SO_4^{*2-} had a calculated CV_C/CV_R <1.

3.2.2. C-R patterns of trace elements, nutrients and Fe and Al

The C-R relationship b-values of Mo are mostly negative or near zero (ranging from 0.07 at Little Wolf to −0.31 at Elkton). Measured trace elements Mo and U had fairly low concentration variability with the exception of Mo at Elkton ($CV_C/CV_R > 1$). The concentration-runoff relationship of K^{+*} was similar to SiO_2 with b-values closest to zero and $CV_C/CV_R < 1$. In contrast, the C-R relationships of NO_3^- are generally positive, with the exception at Little Wolf (b = −0.09), while the CV_C/CV_R of NO_3^- varies between low and high concentration variability. Phosphate did not have a consistent behavior represented by its b-value, ranging from b = −0.32 at Elkton to 1.09 at Van Duzen. Its CV_C/CV_R varied widely (Appendix A Table S4). Concentration-runoff relationship b-values for Fe and Al are positive at all tributaries and have CV_C/CV_R values > 1 indicating highly chemodynamic behavior.

3.3. Storm Plots

Data was collected at Little Wolf Creek and at Elkton during a storm event for high resolution analysis of changes in elemental concentration as a function of runoff. At both of these Umpqua locations, only half of the hydrograph was sampled, and as such any potential hysteresis could not be evaluated. The storm data collected for Little Wolf did not capture the beginning of the event, but there is high resolution data for the peak and falling limb of the hydrograph. From the middle of the falling limb of the storm Ca^{2+*}, Mg^{2+*}, Na^{+*}, Re, SiO_2, and SO_4^{2-*} all have a slight increase in concentration with decreasing runoff (Appendix A Fig. S4). In contrast, anions and K^{+*} concentrations decrease as runoff decreases. Rhenium showed contrasting behavior to other trace elements, like Mo and U. During the falling limb of the storm hydrograph at Little Wolf Creek, Re concentrations gradually increased, while Mo and U concentration decreased. Iron and Al concentrations during the falling limb are also unlike Re and more similar to Mo and U (Appendix A Fig. S4)).

At Elkton, the data collected captures only the rising limb of a storm event up to the peak discharge. Rhenium concentration decreases with increasing runoff, similar to silicate weathering products like Ca^{2+*} and Na^{+*}. The concentrations of Mg^{2+*}, SO_4^{2-*}, and Mo remain fairly constant through the rising limb of the storm. Unlike at Little Wolf, anions behave differently from one another. Phosphate concentrations decrease with increasing runoff, and U, K^{+*}, Mo, and NO_3^- concentrations increase through the rising limb of the storm. In the Elkton storm event, Fe and Al concentrations increase with increasing runoff (Appendix A Fig. S4).

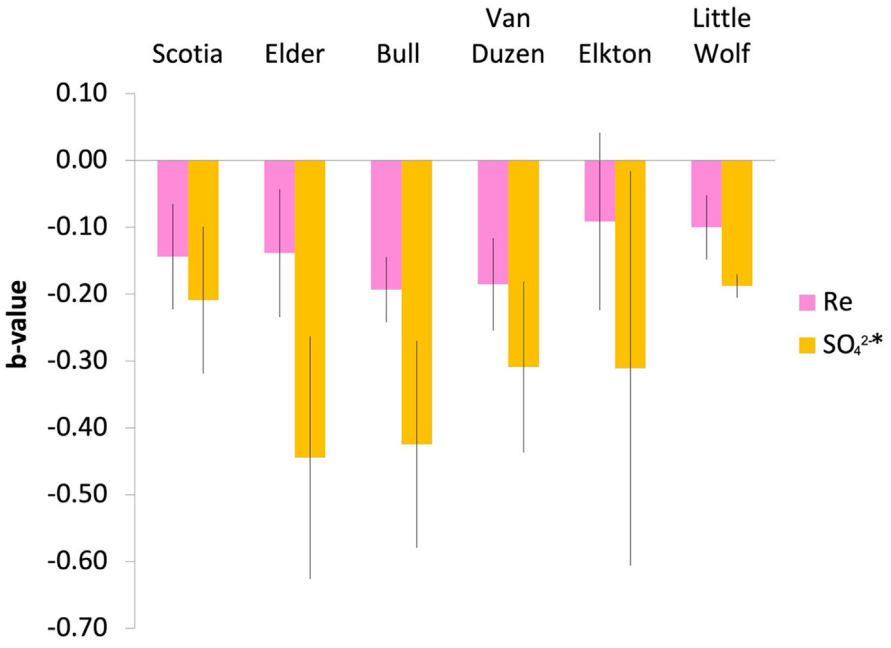

Fig. 4. Comparison of the calculated b-value of Re and SO_4^* at all tributaries with significant p values for these C-R relationships. Uncertainties on b-values represent the 95% confidence interval.

In the Eel River basin, stormwater sampling captured both the rising and falling limb of the hydrograph at four locations: Scotia, Elder Creek, Bull Creek, and Van Duzen. At all four sites SO_4^{2-*} undergoes greater dilution with increasing runoff compared to Re (Fig. 5). While there is a contrast in the steepness of dilution between Re and SO_4^{2-*} at Scotia, the difference is smaller than at Elder Creek, Bull Creek, or Van Duzen (Appendix A Table S5). During the storm event at all four Eel river basin sites, Re behaves most similarly to Ca^{2+*} and Na^{+*}. Concentrations of these solutes decrease with increasing runoff until the peak of the event, when concentrations begin to stabilize with decreasing runoff (Fig. 5 and Appendix A Fig. S5). In contrast, Fe and NO_3^- concentrations show very different and much more chemodynamic behavior during the storm event as compared to Re (Fig. 5 and Appendix A Fig. S5). Rhenium also shows distinct behavior from Mo, U, K^{+*}, and Al during the storm event at the four Eel River basin sites (Appendix A Fig. S5).

3.4. Sediment Yield

Available sediment yield data from the Umpqua River at Elkton (Curtiss, 1975; Wise and O'Connor, 2016) are consistent with long-term erosion rates based on ^{10}Be (Balco et al., 2013). We observe a positive correlation between dissolved mean solute concentrations and suspended sediment yield (Appendix A Table S4). In contrast, there was no observed relationship between average basin slope, mean annual precipitation, mean annual temperature (Table 1) and mean solute concentration (Appendix A Table S3), although the overall variation in these variables across the Eel and Umpqua Basins was somewhat limited. Likewise, there was no correlation of a-values or b-values with drainage basin area. While suspended sediment yields are highly variable on a yearly basis, dissolved solute C-R patterns tend not to vary much through time, unless anthropogenically influenced (Godsey et al., 2019; Torres and Baronas, 2021; Warrick et al., 2013). The comparison of dissolved

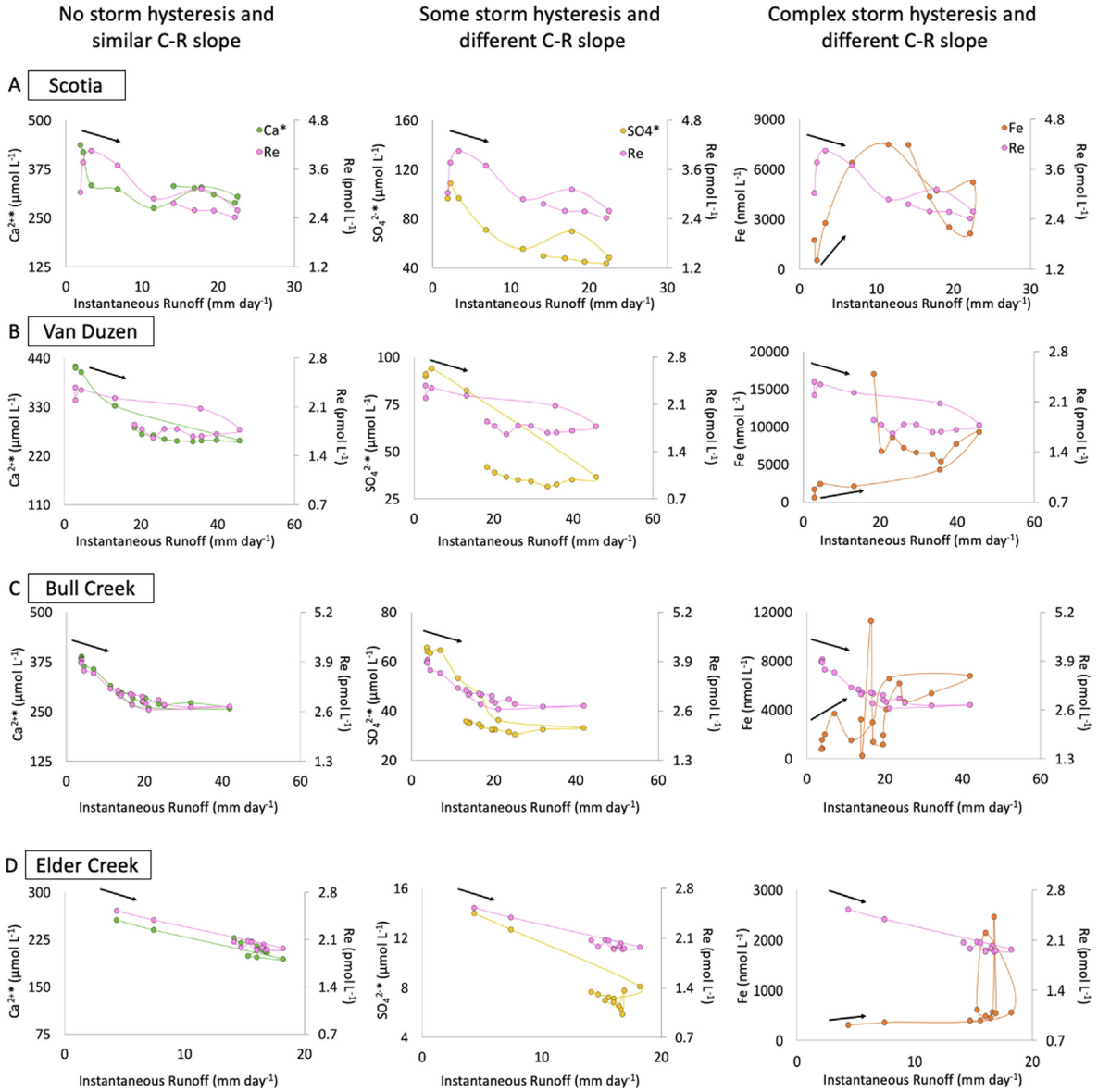

Fig. 5. Storm plots showing concentration-runoff behavior for SO_4^{2-*}, Ca^{2+*}, and Fe relative to Re. Each row of panels (A–D) represents a particular sampling location, and each column is a specific hysteresis behavior Both the right and left y-axis scale ranges are always a factor of 4, with the exception of Fe , which has a wider range of concentration variability.

solute data from this study and historical USGS and DEQ data (Appendix A Fig. S1) yielded similar results in mean concentration and b-values of C-R relationships (Section 3.2) allowing for comparison with previously collected solute data.

4. Discussion

In this section, we evaluate the dissolved chemistry and constrain the source of Re with respect to other sources of solutes in the dissolved load of the Eel and Umpqua rivers, including: weathering products derived from sulfide mineral oxidation, other trace elements released during weathering, nutrients from the riparian zone, colloidal sourced solutes, and primary weathering products from bedrock minerals. In this comparison, we establish that dissolved Re concentrations in both the Eel and Umpqua Rivers behave distinctly from those of SO_4^{2-*} derived from sulfide weathering. Instead, Re behaves most similarly to weathering products derived from bedrock silicate and carbonate primary minerals. This suggests that for Re and primary weathering-derived solutes, the rates at which they are supplied, the depth ranges in the weathering zone from which they are supplied, and/or the processes controlling their supply are similar. Next, we establish that dissolved Re concentration correlates with erosion rate through two comparisons: (1) between the Eel and Umpqua Rivers and (2) as a paired-catchment study between Bull Creek and Elder Creek in the Eel River. The characterization of dissolved Re in this study suggests that the release of Re, presumably from OC_{petro} oxidation, occurs concomitantly with the weathering of primary silicate and carbonate bedrock minerals. Therefore, Re is likely a viable tracer for geo-respiration, as opposed to being dominantly supplied from sulfide oxidation.

4.1. Identifying the source of dissolved Re

4.1.1. Sulfide oxidation

The weathering of reduced sediments, such as OC_{petro} and sulfide minerals, is thought to be the main source of Re as the soluble oxyanion ReO_4^- to the dissolved load of rivers around the world (Dalai et al., 2002; Dellinger et al., 2021; Horan et al., 2019). Both OC_{petro} and sulfide minerals are often present in the same marine sedimentary environments and are brought to the surface during tectonic uplift, weathering, and erosion of sedimentary and metasedimentary rocks (Berner and Raiswell, 1983; Sheen et al., 2018). The observed correlation between dissolved Re and SO_4^{2-*} in compilations of river chemistry could be interpreted two ways. In one scenario, Re found in the dissolved chemical load could be from the release of trace Re hosted in sulfide minerals that is released upon oxidative weathering. Alternatively, because the nature of sulfide mineral and organic carbon burial and preservation is similar, the correlation between dissolved Re and SO_4^{2-*} could simply reflect that in a global database of lithologies, the rocks that tend to have higher sulfide content are the same rocks that may also have higher OC_{petro} content, and the Re may be predominantly associated with that OC_{petro}. Solely comparing trends between concentrations of dissolved chemical species across many rivers is also inconclusive given that dissolved solute concentrations in rivers are simultaneously controlled by changes in evaporation and dilution once weathered from bedrock (Gaillardet et al., 1999).

In order to constrain the sources of dissolved Re and SO_4^{2-*}, we first identified the potential lithologic and atmospheric sources. The Eel River basin is dominated by metasedimentary silicate rocks with trace amounts of carbonate minerals, while the Umpqua River basin hosts sedimentary and metasedimentary rocks with trace carbonate minerals, as well as Cascades volcanic rocks (Table 1) (Langenheim et al., 2013; Walker and MacLeod, 1991). There is no evidence of evaporite rocks in either basin, and the land use is not consistent with significant SO_4^{2-} fertilizer usage, suggesting that dissolved SO_4^{2-*} (which is already corrected for atmospheric inputs) in these rivers is dominantly derived from the oxidation of trace sulfide phases in the bedrock. For Re, we estimated the potential contribution of rain-derived Re to the river flux. In order to further constrain potential sources of Re contributing to the dissolved chemical load of the Eel and Umpqua Rivers, we measured Re concentrations in local, open-rainfall precipitation (Table 3).

A single rainwater sample collected near Elder Creek in the Eel River basin had a Re concentration of 0.069 pmol/L, while a rainwater sample collected near Ten Mile in the Umpqua River basin had a Re concentration of 0.20 pmol/L. Based on the measured Re content of rainwater at each location, the mean annual precipitation, and the mean runoff during the water years of our sampling campaigns (2015–2019), a simplistic calculation indicates that rain-derived Re may represent ~4% of the riverine flux in the Eel and ~21% of the Re flux in the Umpqua. More extensive sampling of atmospheric inputs would be needed to better assess this input of Re, which is likely anthropogenic and may be related to coal burning in Asia (Colodner et al., 1995), but is relatively lower than in the global analysis by Miller et al. (2011), which estimated that approximately 30% of Re is sourced from anthropogenic input. Nevertheless, the proportion of Re derived from rainwater to the riverine flux appears to be an important constraint on the global riverine Re budget, based on the very limited data sets available, and is a variable in need of further measurements.

Across all of the sampled tributaries of the Eel and Umpqua Rivers, the storm water plots, power law C-R relationships, and CV_C/CV_R of dissolved Re and SO_4^{2-*} appear to be different (Figs. 4–6, and Appendix A Fig. S4 and Fig. S5). In both the Eel and Umpqua, SO_4^{2-*} undergoes greater dilution with increasing runoff compared to Re. The C-R b-value of SO_4^{2-*} was more negative compared to Re at all 12 tributaries, and at Elder Creek, Bull Creek and Little Wolf, there is no overlap of the b-values of Re and SO_4^{2-*} within the 95% confidence interval (Appendix A Table S4 and Table S5). The b-value of Re varies between −0.09 at Elkton to −0.19 at both Bull Creek and Elder Creek. The b-value of SO_4^{2-*} ranges between −0.19 at Little Wolf to −0.44 at Elder Creek. The C-R behavior of Re and SO_4^{2-*} showed distinct slopes and intercepts among the different physiographic regions within the Eel and Umpqua (Fig. 6), but the steeper negative slope of SO_4^{2-*} as compared to Re remained an overarching feature.

The more negative b-values of SO_4^{2-*} in both the Eel and Umpqua are consistent with sulfide oxidation occurring at a faster rate than other bedrock minerals, and at a deeper depth within the weathering profile (Gu et al., 2020b; Kanzaki et al., 2020;

Table 3
Measured Re rainwater data.

Watershed	Location	Sampling Dates	Re (pmol L^{-1})	Watershed precipitation Re flux (kg yr^{-1})	Watershed river Re flux (kg yr^{-1})	Contribution of rainwater Re to riverine Re flux (%)
Eel	Elder Creek	11/2018	0.069	0.16	3.68	4.4
Umpqua	Ten Mile	12/2018	0.20	0.46	2.15	21

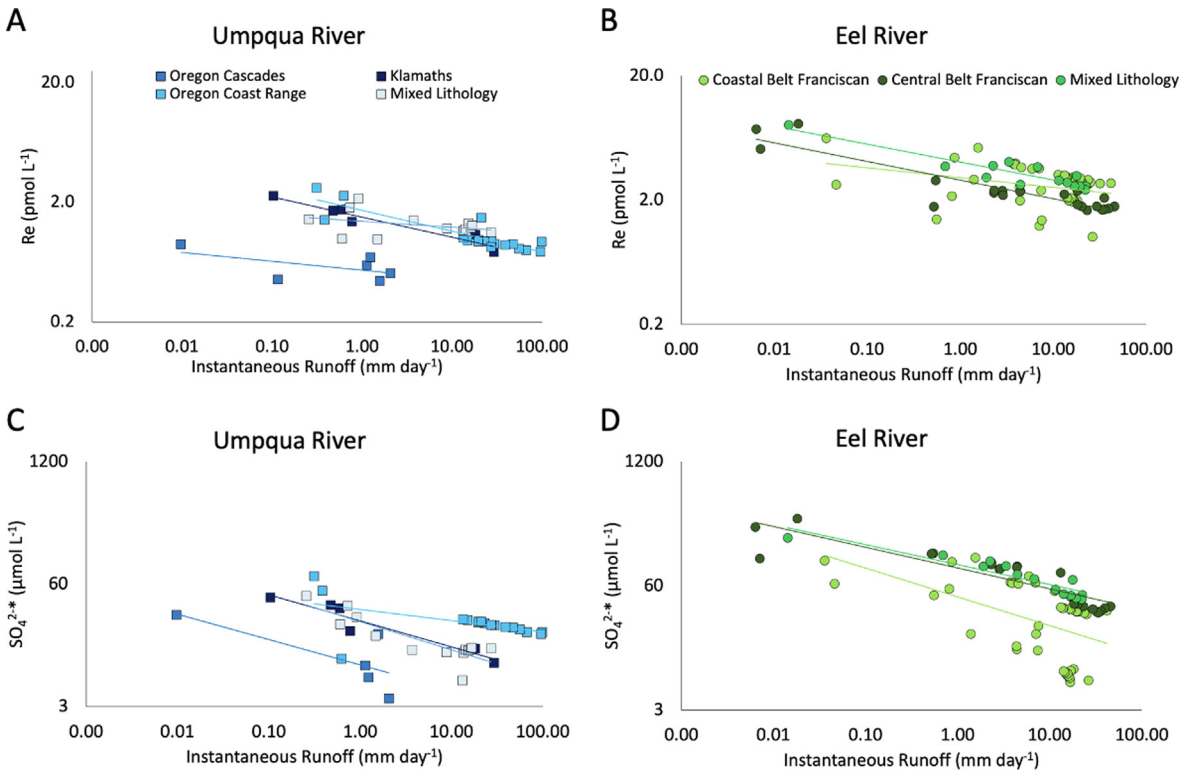

Fig. 6. Concentration-runoff relationship of Re in tributaries of the three physiographic regions of the Umpqua River Basin (Oregon Cascades, Klamaths, and Oregon Coast Range) and an additional category of tributaries mixing waters draining from the Oregon Cascades and the Oregon Coast Range (A) and in tributaries of the two physiographic regions of the Eel River Basin (Coastal Belt Franciscan and Central Belt Franciscan) and an additional category of tributaries mixing waters draining from the Coastal Belt Franciscan and from the Central Belt Franciscan (B). Concentration-runoff relationship of SO_4^* in tributaries of the three physiographic regions of the Umpqua River Basin (Oregon Cascades, Klamaths, and Oregon Coast Range) and an additional category of tributaries mixing waters draining from the Oregon Cascades and the Oregon Coast Range (C) and in tributaries of the two physiographic regions of the Eel River Basin (Coastal Belt Franciscan and Central Belt Franciscan) and an additional category of tributaries mixing waters draining from the Coastal Belt Franciscan and from the Central Belt Franciscan (D).

Winnick et al., 2017). This in turn means that with increasing runoff, the concentration of SO_4^{2-*} becomes more strongly diluted because when the water table rises above the sulfide weathering front, SO_4^{2-*} becomes supply limited. In addition, the CV_C/CV_R relationship of SO_4^{2-*} at all tributaries show that SO_4^{2-*} is more chemodynamic than Re in all 6 watersheds for which more than four samples were available (Fig. 7).

4.1.2. Trace elements

We next compare the C-R relationship and CV_C/CV_R of Re with the trace elements Mo and U. Uranium can be present as a trace constituent in many primary minerals and in accessory phases. Uranium is also known to be affected by sorption on secondary minerals and organic matter, while Mo and Re are both hosted primarily in organic carbon and some sulfides (Greeman, 1992; Helz and Dolor, 2012; King et al., 2018; Miller et al., 2011; Morford and Emerson, 1999; Morton et al., 2001). The storm water C-R behavior of trace elements like Mo and U differ from that of Re, with the details of the deviation depending on the tributary (Appendix A Fig. S5). Uranium mostly exhibits counter-clockwise hysteresis, which suggests there is a delayed source or lagged through-flow response in the delivery of the species to the dissolved load. Meanwhile the behavior of Mo varies between counter-clockwise hysteresis and figure eight hysteresis. The latter is observed when the ratio of concentration to runoff is greater during the rising limb of the event relative to the ratio during the falling limb at the same runoff values (Arora et al., 2020; Rose et al., 2018). The complex C-R hysteresis pattern in the concentration-runoff plots of Mo has been observed previously in the East River in Colorado, USA (Arora et al., 2020). In Fig. 5, we observe an absence of Re hysteresis during the course of the storm event. Scotia, Van Duzen, Elder Creek, and Little Wolf, the b-values of Mo, U, and Re are similar, but U and Mo differ from Re in their chemostatic vs chemodynamic behavior (Appendix A Fig. S6). Elkton, in contrast, shows difference between all three trace elements with respect to the b-value and CV_C/CV_R (Appendix A Table S4 and Fig. S6). Given the difference in the behavior of Mo and U from Re, it is not likely Re is released from the same dominant sources, flowpaths, and/or processes as these two elements. The affinity of these trace metals for secondary phases may offer an explanation for their contrasting C-R behavior. A previous study of Re behavior during weathering found that Re was not fixed into secondary Fe-oxide phases that precipitated in weathering profiles (Pierson-Wickmann et al., 2002), which contrasts with Mo and U are both known to be incorporated into secondary Fe-oxide phases during weathering (Goldberg et al., 1996; Pett-Ridge et al., 2007).

4.1.3. Nutrients

We next compare the behavior of Re to nutrients, like K^{+*}, NO_3^-, and PO_4^{3-}. The mechanisms for solute generation of these three species are different, but all are heavily biologically cycled. Nitrate is dominantly sourced from mineralization in surface soils and riparian zones, and the supply of available phosphate is controlled mostly by the chemical weathering of apatite. The supply of K is controlled by both silicate primary mineral dissolution, such as feldspars and mica, and mobilization of biologically cycled K from shallow surface soils (Berner and Berner, 2012; Hillel, 2008). Potassium is neither strongly flushed nor strongly diluted during storm events, and its CV_C/CV_R is quite chemostatic. The slopes of the C-R relationships and the near clockwise storm water hysteresis C-R

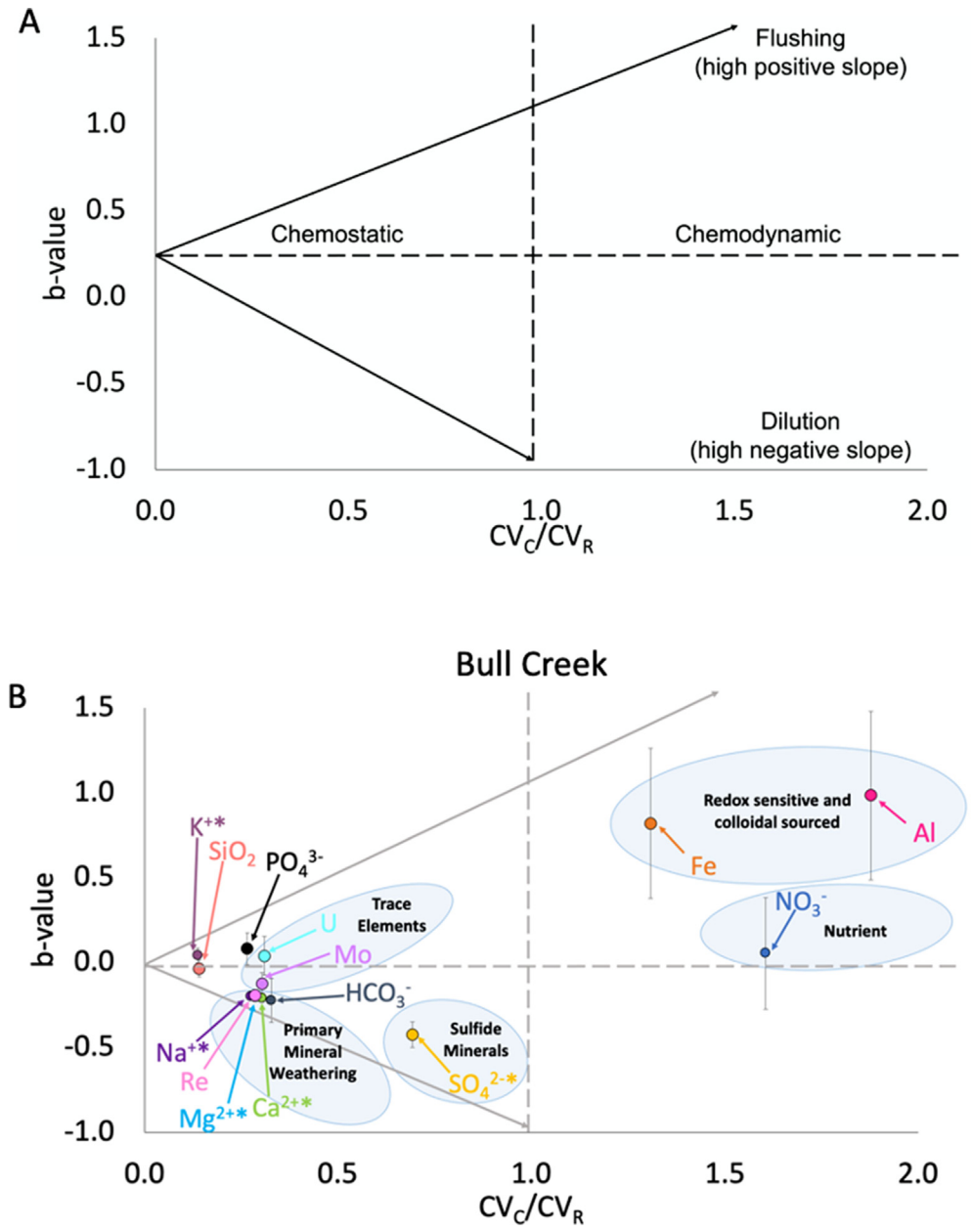

Fig. 7. Ratio of the coefficient of variation of the concentration to the coefficient of variation to the runoff (CV_C/CV_R) plotted against the slope (b-value) of the stream water concentration-runoff relationship for solutes measured in this study. Panel A represents the behavioral domains of the interpretation of weathering behavior from the diagrams. Panel B is the b-value versus CV_C/CV_R for Bull Creek. Vertical bar represents ±1 standard error of b-value.

patterns of NO_3^- and PO_4^{3-} at tributaries in the Eel and Umpqua are consistent with these species being flushed from the riparian zone. We observe that NO_3^- has mostly positive b-values, and ranges from −0.07 at Van Duzen to 0.76 at Elder Creek. The CV_C/CV_R ratios suggest that NO_3^- may behave chemostatically or chemodynamically, depending on the redox conditions of the riparian zone and whether or not it is behaving as a source or sink for N (Rogers et al., 2021), but PO_4^{3-} is fairly chemostatic across all the study locations (Fig. 7 and Appendix A Fig. S6). Phosphate has mostly positive b-values in the Eel, ranging from −0.06 at Elder Creek to 0.21 at Scotia, but mostly negative b-values in the Umpqua, ranging from −0.32 at Elkton to −0.07 at Little Wolf (Appendix A Table S4). The more negative b-values for PO_4^{3-} in the Umpqua may reflect a greater dominance of primary mineral weathering in controlling PO_4^{3-} supply, which may be linked to the P-rich volcanic rocks in the Cascades. The overall decoupling of nutrient behavior from that of Re implies that Re is not predominantly flushed from surface soils in the Eel and Umpqua basins.

4.1.4. Colloids

Riverine samples filtered with a 0.2 μm PES filter yielded lower concentrations of Al and Fe than riverine samples filtered with a 0.8 μm PES filter (Appendix A Fig. S7). This difference in concentration is consistent with Fe and Al being present in colloidal form within the size range from 0.2 μm to 0.8 μm. While this range in filter sizes does not encompass the complete size range of colloidal particles, the partial range allows us to examine whether other solutes show similar colloidal behavior. All other river solutes in this study, including Re, had identical concentrations in samples filters at 0.2 μm and at 0.8 μm. Colloids may be mobilized from

the weathering zone to rivers as a result of hydrologic changes and/or redox processes (King et al., 2019; Neubauer et al., 2013; Thompson et al., 2006). The storm water C-R patterns of Al and Fe are dissimilar from those of Re, and display counter-clockwise hysteresis (Fig. 5 and Appendix A Fig. S5). The b-values of Al and Fe are both positive at all tributaries, and the CV_C/CV_R of Al and Fe are both much more chemodynamic, which is consistent with mobilization of colloids during heavy rainfall events (Fig. 7 and Appendix A Supplementary Material) (Arora et al., 2020; Knapp et al., 2020). Both the contrast in C-R patterns between Re and Fe and Al, as well as the lack of difference between Re concentrations measured in stream samples filtered at 0.2 μm and 0.8 μm, indicate that Re is not mobilized in colloidal form. These observations suggest that Re supply is not dominantly controlled by colloid transport.

4.1.5. Major cations and other weathering derived solutes

Calculated b-values for major cations, SiO_2, and HCO_3^- in the Eel and Umpqua Rivers are consistent with what has been observed in previous studies of rivers elsewhere (Godsey et al., 2009; Herndon et al., 2015; Rose et al., 2018) and in field data globally (e.g. GloRiCh dataset) (Torres and Baronas, 2021). Dissolved SiO_2 is controlled by both primary mineral dissolution and also by secondary mineral precipitation (Berner and Berner, 2012). There is some evidence of solute production resulting from cation exchange occurring in tandem with mineral dissolution in the Eel River at Elder Creek (Kim et al., 2014), but it is likely that primary mineral dissolution drives most major mineral weathering products in these watersheds. Future work could focus on the characterization of primary mineral weathering mechanisms in these watersheds. Overall, the log–log C-R relationships of Re and primary mineral weathering products Ca^{2+*}, Mg^{2+*}, and Na^{+*}, and HCO_3^- are similar (Appendix A Table S4 and Fig. S8).

The slope of the C-R relationship and the CV_C/CV_R of Re, primary weathering products like Ca^{2+*}, Mg^{2+*}, and Na^{+*}, and HCO_3^- all show weak dilution and relatively chemostatic behavior. This behavior is consistent with solutes being derived from equilibration of long residence time porewaters with dissolving minerals (Maher, 2011). From this detailed data set, we can see that Re behaves similarly to Ca^{2+*}, Mg^{2+*}, and Na^{+*}, across all runoff conditions at all tributaries (Table 4), suggesting Re release occurs concomitantly with the dissolution of primary silicate and carbonate bedrock minerals and other materials weathered over a similar depth range. Given the previous evidence that Re is associated with OC_{petro} (Dellinger et al 2021), and that dissolved Re release is derived from OC_{petro} in bedrock (e.g. Colodner et al., 1993), and the fact that that OC_{petro} is present in the bedrock in these specific watersheds (Goñi et al., 2013; Underwood et al., 1988; Blair et al., 2003; Leihold et al., 2006), we suggest that Re release in the Eel and Umpqua watersheds is likely occurring from from OC_{petro} oxidation. The observation that the b-values and CV_C/CV_R of Re are most similar to that of primary silicate and carbonate weathering solutes also raises the possibility that Re is released directly from those primary silicate or carbonate phases, or, more generally speaking, that Re release is occurring at a similar depth range and via similar flowpaths over which cations like Ca^{2+*}, Mg^{2+*}, and Na^{+*} and their counter-anion, HCO_3^-, are being released (Fig. 7).

Few other studies have focused on directly examining the C-R relationship of Re with respect to weathering products. The data from the Eel and Umpqua Rivers are consistent with the limited data available from the Mackenzie River at Tsiigehtchic, Canada (n_{total} = 10) (Horan, 2018; Miller et al., 2011) and from the Whataroa River (n = 5) in the western Southern Alps, New Zealand (Horan et al., 2017). Rhenium C-R relationships from the Ehlenbach (n = 28) and the Vogelbach (n = 30) Swiss Alps catchments, and the East River (n = 20) in Colorado, USA (Hilton et al., 2021) are more complex. In contrast, the C-R relationship of dissolved Re from the Liwu River in Taiwan (n = 2) suggested a positive correlation between Re and runoff (Hilton et al., 2014). It is possible that the observed positive correlation is a result of limited data being available over only a small range of discharge, or there may be some rainfall-derived Re influencing stream concentrations.

4.2. Dissolved Re and erosion rate

Physical erosion is often positively correlated with chemical weathering rates (e.g. Dupré et al., 2003), and to date, field-based observations and quantification of oxidation of OC_{petro} has been limited to a handful of locations that are either subject to extreme erosion rates, including mountainous river catchments in Taiwan (Hilton et al., 2014), New Zealand's Southern Alps (Horan et al., 2017), and the Ganges-Brahmaputra and Yamuna river systems (Dalai et al., 2002; Galy et al., 2008), or the very large river basins of the Amazon (Bouchez et al., 2010) or the Mackenzie in western Canada (Horan et al., 2019). The Eel and Umpqua are small mountainous rivers that offer a contrast to these previously studied rivers in both their geographic size and in their intermediate erosion rate. In Section 4.1, we address the most likely source of dissolved Re in the Eel and Umpqua Rivers being silicate minerals, carbonate minerals, or OC_{petro} embedded in bedrock known to be present in these watersheds (Blair et al., 2003; Goñi et al., 2013; Leithold et al., 2006), and Re appears to be released across similar flowpaths, depth ranges, and/or rates and mechanisms of release as primary mineral weathering. Here we discuss a positive correlation between the observed dissolved Re concentration in the Eel and Umpqua rivers and the erosion rate in the context of the refining the use of Re as a tracer of georespiration.

The average suspended sediment load of the Eel River is almost 15 times greater than that of the Umpqua, moving 2232 tons km^{-2} yr^{-1} versus 147 tons km^{-2} yr^{-1}, respectively (Table 2) as a result of the tectonic setting of the Eel in proximity to the Mendocino Triple Junction (Balco et al., 2013; Blair et al., 2003). There is a marked difference in the mean solute concentrations, wherein almost all mean solute concentrations are greater in the Eel compared to the Umpqua (Fig. 3 and Table 3). We observe a positive correlation in mean concentration of solutes, such as Re, with erosion rate, which suggests that chemical weathering fluxes (e.g. georespiration, carbonate weathering, silicate weathering) in the Eel and Umpqua Rivers co-vary with erosion rate. Some of the differences in concentrations may simply be due to difference in lithology between the Eel and Umpqua basins (Fig. 6). A large fraction of the Umpqua river basin in the Klamath and Cascades is underlain by much less erodible volcanic rock, which likely has little OC_{petro} (Fig. 1), which may explain the lower Re concentrations in these physiographic regions relative to the sedimentary underlain Oregon Coast Range. The Franciscan Formation in the Eel River basin contains significant amounts of petrogenic carbon (Leithold and Blair, 2001), and there are enhanced contributions of mineral sediment that occur during both high and low flows with roughly equal fractions of OC_{petro} and of aged biogenic OM (Goñi et al., 2013). Despite the difference in the thermal maturity of the OC_{petro} between the physiographic regions in the Eel (Underwood et al., 1988), there was no clear difference in Re C-R relationship between the two regions (Appendix A Table S3 and Table S4). In addition to bedrock heterogeneity, the higher erosion and chemical weathering rates in the Eel likely contribute to the elevated Re concentrations in the Eel compared to the Umpqua.

The sub-catchments of Bull Creek and Elder Creek, which are both Coastal Franciscan terrane in the Eel River basin allow for a way to examine the effect of erosion on Re release while holding the lithology relatively constant. These sub-catchments also have similar vegetation and climate, but due to their tectonic setting,

Bull Creek, which is closer to the Mendocino Triple Junction, has an erosion rate that is 3 times greater than the erosion rate at Elder Creek (Willenbring et al., 2013). The dissolved solute concentrations of the faster eroding Bull Creek are greater than that of the Elder Creek (Appendix A Table S3). The Re concentration at mean runoff was ~1.8 times greater at Bull Creek than Elder Creek. The association of higher dissolved Re concentrations at the faster eroding Bull Creek compared to the slower eroding Elder Creek supports the idea that Re release is associated with OC_{petro} in bedrock and that the flux of OC_{petro} oxidation is controlled on a first-order by erosion rate. The OC_{petro} hosted in the bedrock of these two tributaries is similar in terms of thermal maturity (Underwood et al., 1988). It is acknowledged, however, that the bedrock Re/OC_{petro} ratio may vary within and between watersheds. For example, in Switzerland in the Ehrlenbach and Vogelbach, Hilton et al. (2021) found that the bedrock composition was variable, at $3.3 \pm 2.5 \times 10^{-7}$ (1 s.d., n = 8), which is similar to gray shales and sedimentary rocks elsewhere (Dalai et al., 2002; Hilton et al., 2014; Horan et al., 2017; Jaffe et al., 2002). It is possible that there may be some underlying heterogeneity in the lithology between Bull Creek and Elder Creek. Nevertheless, our observation of higher mean Re concentration in the basin with higher sediment yield and erosion rate agrees with what has previously been observed in the Erlenbach and Vogelbach in Switzerland, in the East River of Colorado, the Mackenzie River in Canada, rivers in the Southern Alps of New Zealand, and rivers in Taiwan (Hilton et al., 2014; Hilton et al., 2021; Horan et al., 2019; Horan et al., 2017).

5. Conclusion and Future Work

The sources and mechanisms controlling the release of Re to the dissolved chemical load of the Eel and Umpqua Rivers were assessed using storm water data, C-R relationships, and CV_C/CV_R of different solutes, representing different potential sources to the dissolved chemical load. Comparing dissolved Re and SO_4^{2-*}, we conclude that while trace amounts of Re may be released from sulfide oxidation, the C-R relationship and CV_C/CV_R of Re is chemostatic and has slight dilution with increasing runoff compared to SO_4^{2-*}, which is more chemodynamic and often shows greater dilution with increasing runoff. Therefore, the release of dissolved Re does not trace sulfide oxidation. Given that Re C-R relationships and CV_C/CV_R are most similar to silicate and carbonate weathering products, we conclude that nutrients, colloids, and other trace metals are not the source of Re to the dissolved load. We presume then that the dominant source of Re to the dissolved chemical load is bedrock containing $OC_{petro,}$ where oxidation is limited by available mineral supply. In river waters from the Eel and Umpqua basins, dissolved Re was positively and significantly correlated with the suspended sediment yield, which is a measure of physical erosion rate normalized by runoff. We also observe in a sub-catchment study of the Eel River at Bull Creek and Elder Creek there is a positive relationship between Re concentration and erosion rate, such that systems that erode more rapidly have elevated dissolved Re concentrations relative to systems that have slower erosion rates. This is an important observation on the basis of validating the assumption that links dissolved Re and georespiration because the release of Re is occurring at similar rate of bedrock weathering, meaning its release mirrors the oxidation of OC_{petro} from bedrock as it is brought to the surface. Future work with respect to georespiration will go to studying the weathering profiles in both these watersheds to understand solid phase Re and OC_{petro} dynamics, characterizing the particulate organic carbon mobilized in these watersheds, and constraining the weathering budget of the Eel and Umpqua.

Data availability

Research data associated with this manuscript is provided online in the Hydroshare Repository and in supplementary tables available in the Supplementary Material.

Declaration of Competing Interest

The authors declare that they have no known competing financial interests or personal relationships that could have appeared to influence the work reported in this paper.

Acknowledgements

The research was funded by NSF award EAR – 1655506 awarded to J.C. Pett-Ridge, M. Goñi, and B. Haley. We thank Lin Ma for Sr isotope analyses at the University of Texas at El Paso; Erin Guillory and Jacquelyn Corpus for assisting with field work; Coby Ayers, Callie Covington, and Kylie Welch for assistance with field work and sample preparation; Josef Vincent for assistance with sample preparation; Chris Russo and Beth Rutila for assisting with analyses conducted in the Keck Lab; William Fairchild, Burke Hales, and Joe Jennings for assistance with DIC analyses; and Katherine Worms for assistance in mapping in ArcGIS. Peter Steele is thanked for allowing access to the Angelo Coast Reserve for sampling. Jay Harris is thanked for assistance with permitting for sampling in Humboldt Redwoods State Park. There are no competing interests. We would like to thank reviewers for their thorough reviews and suggestions that improved the quality of this manuscript.

Research data

Research data associated with this article can be accessed at https://www.hydroshare.org/resource/e0981ae53fef43ce94af1dffbb6ab52e/.

Appendix A. Supplementary material

Supplementary material to this article can be found online at https://doi.org/10.1016/j.gca.2022.09.036.

References

Aguilera, R., Melack, J.M., 2018. Concentration-Discharge Responses to Storm Events in Coastal California Watersheds. Water Resour. Res. 54, 407–424.
Ameli, A.A., Beven, K., Erlandsson, M., Creed, I.F., McDonnell, J.J., Bishop, K., 2017. Primary weathering rates, water transit times, and concentration-discharge relations: A theoretical analysis for the critical zone. Water Resour. Res. 53, 942–960.
Anbar, A.D., Creaser, R.A., Papanastassiou, D.A., Wasserburg, G.J., 1992. Rhenium in seawater: Confirmation of generally conservative behavior. Geochim. Cosmochim. Acta 56, 4099–4103.
Arora, B., Burrus, M., Newcomer, M., Steefel, C.I., Carroll, R.W., Dwivedi, D., Dong, W., Williams, K.H., Hubbard, S.S., 2020. Differential CQ Analysis: A New Approach to Inferring Lateral Transport and Hydrologic Transients Within Multiple Reaches of a Mountainous Headwater Catchment. Front. Water 2, 24.
Balco, G., Finnegan, N., Gendaszek, A., Stone, J.O., Thompson, N., 2013. Erosional response to northward-propagating crustal thickening in the coastal ranges of the US Pacific Northwest. Am. J. Sci. 313, 790–806.
Bandstra, L., Hales, B., Takahashi, T., 2006. High-frequency measurements of total CO_2: Method development and first oceanographic observations. Mar. Chem. 100, 24–38.
Bennett, G.L., Miller, S.R., Roering, J.J., Schmidt, D.A., 2016. Landslides, threshold slopes, and the survival of relict terrain in the wake of the Mendocino Triple Junction. Geology 44, 363–366.
Berner, E.K., Berner, R.A., 2012. Global Environment: Water, Air, and Geochemical Cycles. Princeton University Press.
Berner, R.A., Raiswell, R., 1983. Burial of organic carbon and pyrite sulfur in sediments over phanerozoic time: a new theory. Geochim. Cosmochim. Acta 47, 855–862.

Blair, N.E., Leithold, E.L., Ford, S.T., Peeler, K.A., Holmes, J.C., Perkey, D.W., 2003. The persistence of memory: The fate of ancient sedimentary organic carbon in a modern sedimentary system. Geochim. Cosmochim. Acta 67, 63–73.
Bolton, E.W., Berner, R.A., Petsch, S.T., 2006. The weathering of sedimentary organic matter as a control on atmospheric O_2: II. Theoretical modeling. Am. J. Sci. 306, 575–615.
Bouchez, J., Beyssac, O., Galy, V., Gaillardet, J., France-Lanord, C., Maurice, L., Moreira-Turcq, P., 2010. Oxidation of petrogenic organic carbon in the Amazon floodplain as a source of atmospheric CO_2. Geology 38, 255–258.
Brookins, D.G., 1986. Rhenium as analog for fissiogenic technetium: Eh-pH diagram (25°C, 1 bar) constraints. Appl. Geochem. 1, 513–517.
Brookins, D.G., 2012. Eh-pH Diagrams for Geochemistry. Springer Science & Business Media.
Brown, W.M., Ritter, J.R., 1971. Sediment Transport and Turbidity in the Eel River Basin. US Government Printing Office, California.
Chang, S., Berner, R.A., 1999. Coal weathering and the geochemical carbon cycle. Geochim. Cosmochim. Acta 63, 3301–3310.
Cohen, A.S., Coe, A.L., Bartlett, J.M., Hawkesworth, C.J., 1999. Precise Re–Os ages of organic-rich mudrocks and the Os isotope composition of Jurassic seawater. Earth Planet. Sci. Lett. 167, 159–173.
Colodner, D., Sachs, J., Ravizza, G., Turekian, K., Edmond, J., Boyle, E., 1993. The geochemical cycle of rhenium: a reconnaissance. Earth Planet. Sci. Lett. 117, 205–221.
Colodner, D., Edmond, J., Boyle, E., 1995. Rhenium in the Black Sea: comparison with molybdenum and uranium. Earth Planet. Sci. Lett. 131, 1–15.
Copard, Y., Amiotte-Suchet, P., Di-Giovanni, C., 2007. Storage and release of fossil organic carbon related to weathering of sedimentary rocks. Earth and Planetary Science Letters 258, 345–347.
Curtiss, D.A., 1975. Sediment Yields of Streams in the Umpqua River Basin. US Geological Survey, Oregon.
Dalai, T.K., Singh, S.K., Trivedi, J., Krishnaswami, S., 2002. Dissolved rhenium in the Yamuna River System and the Ganga in the Himalaya: Role of black shale weathering on the budgets of Re, Os, and U in rivers and CO_2 in the atmosphere. Geochim. Cosmochim. Acta 66, 29–43.
Danish, M., Tripathy, G.R., Mitra, S., Rout, R.K., Raskar, S., 2021. Non-conservative removal of dissolved rhenium from a coastal lagoon: Clay adsorption versus biological uptake. Chem. Geol. 580, 120378.
Dellinger, M., Hilton, R.G., Nowell, G.M., 2021. Fractionation of rhenium isotopes in the Mackenzie River basin during oxidative weathering. Earth Planet. Sci. Lett. 573, 117131.
Dolor, M.K., Gilmour, C.C., Helz, G.R., 2009. Distinct Microbial Behavior of Re Compared to Tc: Evidence Against Microbial Re Fixation in Aquatic Sediments. Geomicrobiol J. 26, 470–483.
Dupré, B., Dessert, C., Oliva, P., Goddéris, Y., Viers, J., François, L., Millot, R., Gaillardet, J., 2003. Rivers, chemical weathering and Earth's climate. C.R. Geosci. 335, 1141–1160.
Ernst, W.G., 2011. Accretion of the Franciscan Complex attending Jurassic-Cretaceous geotectonic development of northern and central California. GSA Bulletin 123, 1667–1678.
Evans, C., Davies, T.D., 1998. Causes of concentration/discharge hysteresis and its potential as a tool for analysis of episode hydrochemistry. Water Resour. Res. 34, 129–137.
Fuller, T.K., Perg, L.A., Willenbring, J.K., Lepper, K., 2009. Field evidence for climate-driven changes in sediment supply leading to strath terrace formation. Geology 37, 467–470.
Gaillardet, J., Dupré, B., Louvat, P., Allègre, C.J., 1999. Global silicate weathering and CO_2 consumption rates deduced from the chemistry of large rivers. Chem. Geol. 159, 3–30.
Galy, V., France-Lanord, C., Lartiges, B., 2008. Loading and fate of particulate organic carbon from the Himalaya to the Ganga-Brahmaputra delta. Geochim. Cosmochim. Acta 72, 1767–1787.
Galy, V., Peucker-Ehrenbrink, B., Eglinton, T., 2015. Global carbon export from the terrestrial biosphere controlled by erosion. Nature 521, 204–207.
Godsey, S.E., Kirchner, J.W., Clow, D.W., 2009. Concentration–discharge relationships reflect chemostatic characteristics of US catchments. Hydrol. Process.: Int. J. 23, 1844–1864.
Godsey, S.E., Hartmann, J., Kirchner, J.W., 2019. Catchment chemostasis revisited: Water quality responds differently to variations in weather and climate. Hydrol. Process. 33, 3056–3069.
Goldberg, S., Forster, H., Godfrey, C., 1996. Molybdenum adsorption on oxides, clay minerals, and soils. Soil Sci. Soc. Am. J. 60, 425–432.
Goñi, M.A., Hatten, J.A., Wheatcroft, R.A., Borgeld, J.C., 2013. Particulate organic matter export by two contrasting small mountainous rivers from the Pacific Northwest, USA. J. Geophys. Res. Biogeosci. 118, 112–134.
Greeman, D.J., 1992. The Geochemistry of Uranium, Thorium, and Radium in Soils of the Eastern United States. The Pennsylvania State University.
Gu, X., Heaney, P.J., Reis, F.D.A.A., Brantley, S.L., 2020a. Deep abiotic weathering of pyrite. Science 370, eabb8092.
Gu, X., Rempe, D.M., Dietrich, W.E., West, A.J., Lin, T.-C., Jin, L., Brantley, S.L., 2020b. Chemical reactions, porosity, and microfracturing in shale during weathering: The effect of erosion rate. Geochim. Cosmochim. Acta 269, 63–100.
Hatten, J.A., Goñi, M.A., Wheatcroft, R.A., 2012. Chemical characteristics of particulate organic matter from a small, mountainous river system in the Oregon Coast Range, USA. Biogeochemistry 107, 43–66.
Helz, G.R., Dolor, M.K., 2012. What regulates rhenium deposition in euxinic basins? Chem. Geol. 304–305, 131–141.
Hemingway, J.D., Hilton, R.G., Hovius, N., Eglinton, T.I., Haghipour, N., Wacker, L., Chen, M.-C., Galy, V.V., 2018. Microbial oxidation of lithospheric organic carbon in rapidly eroding tropical mountain soils. Science 360, 209–212.
Herndon, E., Dere, A., Sullivan, P., Norris, D., Reynolds, B., Brantley, S.L., 2015. Biotic controls on solute distribution and transport in headwater catchments. Hydrol. Earth Syst. Sci. Discuss. 12.
Hillel, D., 2008. 11. Soil Fertility and Plant Nutrition. In: Hillel, D. (Ed.), Soil in the Environment. Academic Press, San Diego, pp. 151–162.
Hilton, R.G., Turowski, J.M., Winnick, M., Dellinger, M., Schleppi, P., Williams, K.H., Lawrence, C.R., Maher, K., West, M., Hayton, A., 2021. Concentration-Discharge Relationships of Dissolved Rhenium in Alpine Catchments Reveal Its Use as a Tracer of Oxidative Weathering. Water Resour. Res. 57, e2021WR029844.
Hilton, R.G., Gaillardet, J., Calmels, D., Birck, J.-L., 2014. Geological respiration of a mountain belt revealed by the trace element rhenium. Earth Planet. Sci. Lett. 403, 27–36.
Hilton, R.G., West, A.J., 2020. Mountains, erosion and the carbon cycle. Nat. Rev. Earth Environ. 1, 284–299.
Hoagland, B., Russo, T.A., Gu, X., Hill, L., Kaye, J., Forsythe, B., Brantley, S.L., 2017. Hyporheic zone influences on concentration-discharge relationships in a headwater sandstone stream. Water Resour. Res. 53, 4643–4667.
Horan, K., 2018. The oxidative weathering of organic matter and its carbon dioxide emissions: Insights from the trace elements rhenium and molybdenum Doctoral dissertation. Durham University.
Horan, K., Hilton, R.G., Selby, D., Ottley, C.J., Gröcke, D.R., Hicks, M., Burton, K.W., 2017. Mountain glaciation drives rapid oxidation of rock-bound organic carbon. Sci. Adv. 3, e1701107.
Horan, K., Hilton, R.G., Dellinger, M., Tipper, E., Galy, V., Calmels, D., Selby, D., Gaillardet, J., Ottley, C.J., Parsons, D.R., 2019. Carbon dioxide emissions by rock organic carbon oxidation and the net geochemical carbon budget of the Mackenzie River Basin. Am. J. Sci. 319, 473–499.
Husson, J.M., Peters, S.E., 2017. Atmospheric oxygenation driven by unsteady growth of the continental sedimentary reservoir. Earth and Planetary Science Letters 460, 68–75.
Hynicka, J.D., Pett-Ridge, J.C., Perakis, S.S., 2016. Nitrogen enrichment regulates calcium sources in forests. Glob. Change Biol. 22, 4067–4079.
Jaffe, L.A., Peucker-Ehrenbrink, B., Petsch, S.T., 2002. Mobility of rhenium, platinum group elements and organic carbon during black shale weathering. Earth Planet. Sci. Lett. 198, 339–353.
Kanzaki, Y., Brantley, S.L., Kump, L.R., 2020. A numerical examination of the effect of sulfide dissolution on silicate weathering. Earth Planet. Sci. Lett. 539, 116239.
Karlin, R., 1980. Sediment sources and clay mineral distributions off the Oregon coast. J. Sediment. Res. 50, 543–559.
Keller, C.K., Bacon, D.H., 1998. Soil respiration and georespiration distinguished by transport analyses of vadose CO_2, $^{13}CO_2$, and $^{14}CO_2$. Glob. Biogeochem. Cycles 12, 361–372.
Kim, H., Bishop, J.K.B., Dietrich, W.E., Fung, I.Y., 2014. Process dominance shift in solute chemistry as revealed by long-term high-frequency water chemistry observations of groundwater flowing through weathered argillite underlying a steep forested hillslope. Geochim. Cosmochim. Acta 140, 1–19.
Kim, H., Dietrich, W.E., Thurnhoffer, B.M., Bishop, J.K., Fung, I.Y., 2017. Controls on solute concentration-discharge relationships revealed by simultaneous hydrochemistry observations of hillslope runoff and stream flow: The importance of critical zone structure. Water Resour. Res. 53, 1424–1443.
King, E.K., Perakis, S., Pett-Ridge, J.C., 2018. Molybdenum isotope fractionation during adsorption to organic matter. Geochim. Cosmochim. Acta 222, 584–598.
King, E., Thompson, A., Pett-Ridge, J., 2019. Underlying lithology controls trace metal mobilization during redox fluctuations. Sci. Total Environ. 665, 1147–1157.
Knapp, J.L.A., von Freyberg, J., Studer, B., Kiewiet, L., Kirchner, J.W., 2020. Concentration–discharge relationships vary among hydrological events, reflecting differences in event characteristics. Hydrol. Earth Syst. Sci. 24, 2561–2576.
Kučera, J., Kučera, J., Byrne, A., Byrne, A., Mizera, J., Mizera, J., Lučaníková, M., Lučaníková, M., Řanda, Z., Řanda, Z., 2006. Development of a radiochemical neutron activation analysis procedure for determination of rhenium in biological and environmental samples at ultratrace level. J. Radioanal. Nucl. Chem. 269, 251–257.
Langenheim, V., Jachens, R.C., Wentworth, C.M., McLaughlin, R.J., 2013. Previously unrecognized regional structure of the Coastal Belt of the Franciscan Complex, northern California, revealed by magnetic data. Geosphere 9, 1514–1529.
Leithold, E.L., Blair, N.E., 2001. Watershed control on the carbon loading of marine sedimentary particles. Geochim. Cosmochim. Acta 65, 2231–2240.
Leithold, E.L., Blair, N.E., Perkey, D.W., 2006. Geomorphologic controls on the age of particulate organic carbon from small mountainous and upland rivers. Glob. Biogeochem. Cycles 20, GB3022.
Lock, J., Kelsey, H., Furlong, K., Woolace, A., 2006. Late Neogene and Quaternary landscape evolution of the northern California Coast Ranges: Evidence for Mendocino triple junction tectonics. Geol. Soc. Am. Bull. 118, 1232–1246.
Longbottom, T.L., Hockaday, W.C., 2019. Molecular and isotopic composition of modern soils derived from kerogen-rich bedrock and implications for the global C cycle. Biogeochemistry 143, 239–255.

Mackey, B.H., Roering, J.J., 2011. Sediment yield, spatial characteristics, and the long-term evolution of active earthflows determined from airborne LiDAR and historical aerial photographs, Eel River, California. Bulletin 123, 1560–1576.
Maher, K., 2011. The role of fluid residence time and topographic scales in determining chemical fluxes from landscapes. Earth Planet. Sci. Lett. 312, 48–58.
Maher, K., Chamberlain, C., 2014. Hydrologic regulation of chemical weathering and the geologic carbon cycle. Science 343, 1502–1504.
McLennan, S.M., 2001. Relationships between the trace element composition of sedimentary rocks and upper continental crust. Geochem. Geophys. Geosyst. 2.
Miller, C.A., Peucker-Ehrenbrink, B., Walker, B.D., Marcantonio, F., 2011. Re-assessing the surface cycling of molybdenum and rhenium. Geochim. Cosmochim. Acta 75, 7146–7179.
Milliman, J.D., Farnsworth, K.L., 2013. River Discharge to the Coastal Ocean: A Global Synthesis. Cambridge University Press.
Morford, J.L., Emerson, S., 1999. The geochemistry of redox sensitive trace metals in sediments. Geochim. Cosmochim. Acta 63, 1735–1750.
Morton, L., Evans, C., Harbottle, G., Estes, G., 2001. Pedogenic fractionation and bioavailability of uranium and thorium in naturally radioactive spodosols. Soil Sci. Soc. Am. J. 65, 1197–1203.
Musolff, A., Schmidt, C., Selle, B., Fleckenstein, J.H., 2015. Catchment controls on solute export. Adv. Water Resour. 86, 133–146.
Neubauer, E., von der Kammer, F., Knorr, K.-H., Peiffer, S., Reichert, M., Hofmann, T., 2013. Colloid-associated export of arsenic in stream water during stormflow events. Chem. Geol. 352, 81–91.
Omernik, J.M., 1987. Ecoregions of the conterminous United States. Map (scale 1:7,500,000). Ann. Am. Assoc. Geogr. 77, 118–125.
Petsch, S., 2014. Weathering of Organic Carbon 12, 217–238.
Petsch, S., Berner, R., Eglinton, T., 2000. A field study of the chemical weathering of ancient sedimentary organic matter. Org. Geochem. 31, 475–487.
Petsch, S., Eglinton, T., Edwards, K., 2001. ^{14}C-dead living biomass: evidence for microbial assimilation of ancient organic carbon during shale weathering. Science 292, 1127–1131.
Pett-Ridge, J.C., Monastra, V.M., Derry, L.A., Chadwick, O.A., 2007. Importance of atmospheric inputs and Fe-oxides in controlling soil uranium budgets and behavior along a Hawaiian chronosequence. Chem. Geol. 244, 691–707.
Peucker-Ehrenbrink, B., Hannigan, R.E., 2000. Effects of black shale weathering on the mobility of rhenium and platinum group elements. Geology 28, 475–478.
Pierson-Wickmann, A.-C., Reisberg, L., France-Lanord, C., 2002. Behavior of Re and Os during low-temperature alteration: Results from Himalayan soils and altered black shales. Geochim. Cosmochim. Acta 66, 1539–1548.
Rahaman, W., Singh, S.K., Shukla, A.D., 2012. Rhenium in Indian rivers: Sources, fluxes, and contribution to oceanic budget. Geochem. Geophys. Geosyst. 13.
Ramp, L., 1972. Geology & Mineral Resources of Douglas County. State of Oregon, Department of Geology and Mineral Industries, Oregon.
Rogers, D.B., Newcomer, M.E., Raberg, J.H., Dwivedi, D., Steefel, C., Bouskill, N., Nico, P., Faybishenko, B., Fox, P., Conrad, M., 2021. Modeling the impact of riparian hollows on river corridor nitrogen exports. Front. Water 3, 7.
Rooney, A.D., Selby, D., Lewan, M.D., Lillis, P.G., Houzay, J.-P., 2012. Evaluating Re–Os systematics in organic-rich sedimentary rocks in response to petroleum generation using hydrous pyrolysis experiments. Geochim. Cosmochim. Acta 77, 275–291.
Rose, L.A., Karwan, D.L., Godsey, S.E., 2018. Concentration–discharge relationships describe solute and sediment mobilization, reaction, and transport at event and longer timescales. Hydrol. Process. 32, 2829–2844.
Selby, D., Creaser, R.A., 2003. Re–Os geochronology of organic rich sediments: an evaluation of organic matter analysis methods. Chem. Geol. 200, 225–240.
Sheen, A.I., Kendall, B., Reinhard, C.T., Creaser, R.A., Lyons, T.W., Bekker, A., Poulton, S.W., Anbar, A.D., 2018. A model for the oceanic mass balance of rhenium and implications for the extent of Proterozoic ocean anoxia. Geochim. Cosmochim. Acta 227, 75–95.
Soulet, G., Hilton, R.G., Garnett, M.H., Roylands, T., Klotz, S., Croissant, T., Dellinger, M., Le Bouteiller, C., 2021. Temperature control on CO_2 emissions from the weathering of sedimentary rocks. Nat. Geosci. 14, 665–671.
Thompson, S.E., Basu, N.B., Lascurain Jr., J., Aubeneau, A., Rao, P.S.C., 2011. Relative dominance of hydrologic versus biogeochemical factors on solute export across impact gradients. Water Resour. Res. 47.
Thompson, A., Chadwick, O.A., Boman, S., Chorover, J., 2006. Colloid Mobilization During Soil Iron Redox Oscillations. Environ. Sci. Technol. 40, 5743–5749.
Torres, M.A., Baronas, J.J., 2021. Modulation of riverine concentration–discharge relationships by changes in the shape of the water transit time distribution. Global Biogeochem. Cycles 35, e2020GB006694.
Tune, A.K., 2021. Interactions between carbon cycling and bedrock weathering in a forest of the Northwen California Coast Ranges. Doctoral dissertation. University of Texas at Austin.
Underwood, M.B., O'Leary, J., Strong, R., 1988. Contrasts in thermal maturity within terranes and across terrane boundaries of the Franciscan Complex, northern California. J. Geol. 96, 399–415.
Walker, G.W., MacLeod, N.S., 1991. Geologic map of Oregon.
Warrick, J., Madej, M.A., Goñi, M., Wheatcroft, R., 2013. Trends in the suspended-sediment yields of coastal rivers of northern California, 1955–2010. J. Hydrol. 489, 108–123.
Wengel, M., Kothe, E., Schmidt, C.M., Heide, K., Gleixner, G., 2006. Degradation of organic matter from black shales and charcoal by the wood-rotting fungus Schizophyllum commune and release of DOC and heavy metals in the aqueous phase. Sci. Total Environ. 367, 383–393.
Wheatcroft, R.A., Goñi, M.A., Hatten, J.A., Pasternack, G.B., Warrick, J.A., 2010. The role of effective discharge in the ocean delivery of particulate organic carbon by small, mountainous river systems. Limnol. Oceanogr. 55, 161–171.
Wheatcroft, R., Sommerfield, C., 2005. River sediment flux and shelf sediment accumulation rates on the Pacific Northwest margin. Cont. Shelf Res. 25, 311–332.
Wildman, R.A., Berner, R.A., Petsch, S.T., Bolton, E.W., Eckert, J.O., Mok, U., Evans, J.B., 2004. The weathering of sedimentary organic matter as a control on atmospheric O_2: I. Analysis of a black shale. Am. J. Sci. 304, 234–249.
Willenbring, J.K., Gasparini, N.M., Crosby, B.T., Brocard, G., 2013. What does a mean mean? The temporal evolution of detrital cosmogenic denudation rates in a transient landscape. Geology 41, 1215–1218.
Winnick, M.J., Carroll, R.W., Williams, K.H., Maxwell, R.M., Dong, W., Maher, K., 2017. Snowmelt controls on concentration-discharge relationships and the balance of oxidative and acid-base weathering fluxes in an alpine catchment, East River, Colorado. Water Resour. Res. 53, 2507–2523.
Wise, D.R., O'Connor, J., 2016. A Spatially Explicit Suspended-sediment Load Model for Western Oregon. Scientific Investigations Report, Reston, VA, p. 36.
Yang, J.S., 1991. High rhenium enrichment in brown algae: a biological sink of rhenium in the sea? Hydrobiologia 211, 165–170.
Yeghicheyan, D., Bossy, C., Bouhnik Le Coz, M., Douchet, C., Granier, G., Heimburger, A., Lacan, F., Lanzanova, A., Rousseau, T.C.C., Seidel, J.-L., Tharaud, M., Candaudap, F., Chmeleff, J., Cloquet, C., Delpoux, S., Labatut, M., Losno, R., Pradoux, C., Sivry, Y., Sonke, J.E., 2013. A Compilation of Silicon, Rare Earth Element and Twenty-One other Trace Element Concentrations in the Natural River Water Reference Material SLRS-5 (NRC-CNRC). Geostand. Geoanal. Res. 37, 449–467.
Yu, L.L., Fassett, J.D., Guthrie, W.F., 2002. Detection limit of isotope dilution mass spectrometry. Anal. Chem. 74, 3887–3891.